BACHELOR

Study of TU/e grown nanowire single photon detectors

Op het Veld, R.L.M.

Award date:
2012

Study of TU/e grown nanowire single photon detectors

By Roy Op het Veld

Student number: 0677750

23-04-2012 / 31-08-2012

Supervisors:

Döndü Sahin

Prof. dr. Andrea Fiore

1 Abstract

In this project, the first nanowire detectors based on niobium nitride (NbN) films on GaAs grown at TU/e are analyzed to get information about the quality and performance of the devices. The results from these experiments can be used to improve the growth process of the NbN film and also the processing of the nanowires. The yield (percentage of working devices on a sample) is also calculated for every sample.

To do this, the actual widths were measured using SEM . This showed that the actual widths are different from the desired widths. It also showed why several devices were not working. This was caused by broken wires, bad connections between the nanowire and the contact pad or the fact that there was no nanowire at all.

Then, the room temperature resistance was measured, mainly to see if the devices were working. Then, at low temperature, the resistance was measured again, and a characteristic IV curve was made for every working device. From this, the stability of the hotspot could be deduced and also the critical current could be extracted.

Several different methods were then used to perform a statistical analysis on the devices. These methods were compared to see, for example, if there are any local constrictions in the nanowires and how many. The analysis will also show how much difference there is between the nanowires on the same sample, but also between the different samples. The effect of the growth temperature during the growth of the NbN film and the thickness of the NbN layer are being analyzed.

Another analysis showed that there are quite some differences in the contamination levels of the samples.

The optical measurements performed were insufficient to say anything about the quality of the different devices or the performance of the devices. However, they did show that the narrow nanowires are working properly and can be used as single photon detectors. With the help of the simulations it is also clarified that the wide nanowires are indeed latching and are not suitable as single photon detectors in this configuration. A series inductance with the nanowire might resolve this latching issue.

A last remark is that extra measurements are required to get more and better information about the optical quality and performance of these nanowires. There was simply not enough time to perform extra measurements of this sort within the scope of this project.

Table of contents

2 Introduction: Superconducting single photon detectors

2.1 Motivation

Companies are always trying to make their products the best in the market. This can be done by either making their products smaller, faster, cheaper, more durable, etc. When a new method or technology is found, it is important that the communication about the subject stays hidden from competitors. But in a world where the internet is freely available to most people, this is easier said than done. Since it is the knowledge or information on how to build a certain technology that is important, this has to be protected. One way to obtain a secure communication about such sensitive information can be found in quantum cryptography. Quantum cryptography performs cryptographic tasks or breaks cryptographic systems by using quantum mechanical effects.

Quantum key distribution for example is a method to guarantee completely secured communication by using quantum mechanics. It uses the fact that by measuring quantum data, it disturbs that data, so it can only be read once. [16] Photons are very suitable for this form of quantum communication due to their low decoherence.

In practice, there are however a lot of limitations, like impurities in the optical fibers, the connection between the optical fiber and the detector, the bending of the fibers, etc. However, one main limitation for quantum communication at telecom wavelength is the detection efficiency of the detectors. This is where the research to superconducting nanowire single photon detectors (SSPD) started. The first SSPD was developed at Moscow State Pedagogical University in 2001 [14, 15]. To explain how SSPDs work, every part on itself has to be understood, starting with superconductivity.

Superconductivity is a property or state of a material that is reached when the material reaches a temperature below the critical temperature and a current below critical current. Both critical temperature and critical current are the points where the material switches between the normal and superconducting state. When a material is in a superconducting state, it has zero electrical resistance and a current can flow freely through the material. In superconducting state, external magnetic fields are completely expelled from the material due to currents that start flowing near the surface of the material. These currents create a magnetic field that cancels out the external magnetic field. This effect is called the Meissner effect. This is why superconductivity is an electromagnetic phenomenon. Superconducting materials can be classified by their magnetic properties. Type I superconductors have one critical point below which they do not allow magnetic fields inside the material and consist of only one (pure) material. Type II superconductors have two transitions between which they allow some magnetic field inside the material and are impure or compound materials. Niobium nitride (NbN) is an example of a type II superconductor due to its compound buildup.

2.2 Operation principle

The properties and the effects of switching between normal and superconducting state are used in SSPDs to detect photons and sensed as a voltage drop in the electrical circuit. When the material has a temperature lower than the critical temperature, with a bias current just below the critical current, and a photon of energy $h\nu$ interacts with the material, the energy of the photon will be absorbed by a Cooper pair [1] (which is a two-electron pair) and create a high-energy quasi-electron. It will lose its high energy by electron scattering (e^- - e^- interaction), causing an avalanche of quasi-electrons from other

broken Cooper pairs. When the average energy of the quasi-electrons around the energy required breaking a Cooper pair, the interaction between the quasi-electrons and phonons will become dominant (e^- - phonon interaction). This means that the energy of the quasi-electron is being dissipated as heat in the material. This heating of the material can cause the creation of vortex-antivortex pairs [1,2]. This causes a small resistance "spot in the nanowire.

The bias current now tries to avoid the hotspot and gets expelled to the sidewalks of the nanowire. This causes the current density at the sidewalks to increase and become larger than the critical current density (see figure 1). In consequence of that, these parts of the wire become resistive as well. Now, a part of the nanowire is completely resistive, causing a sudden increase at the load resistance (R_L) that can be measured indirectly. [1]

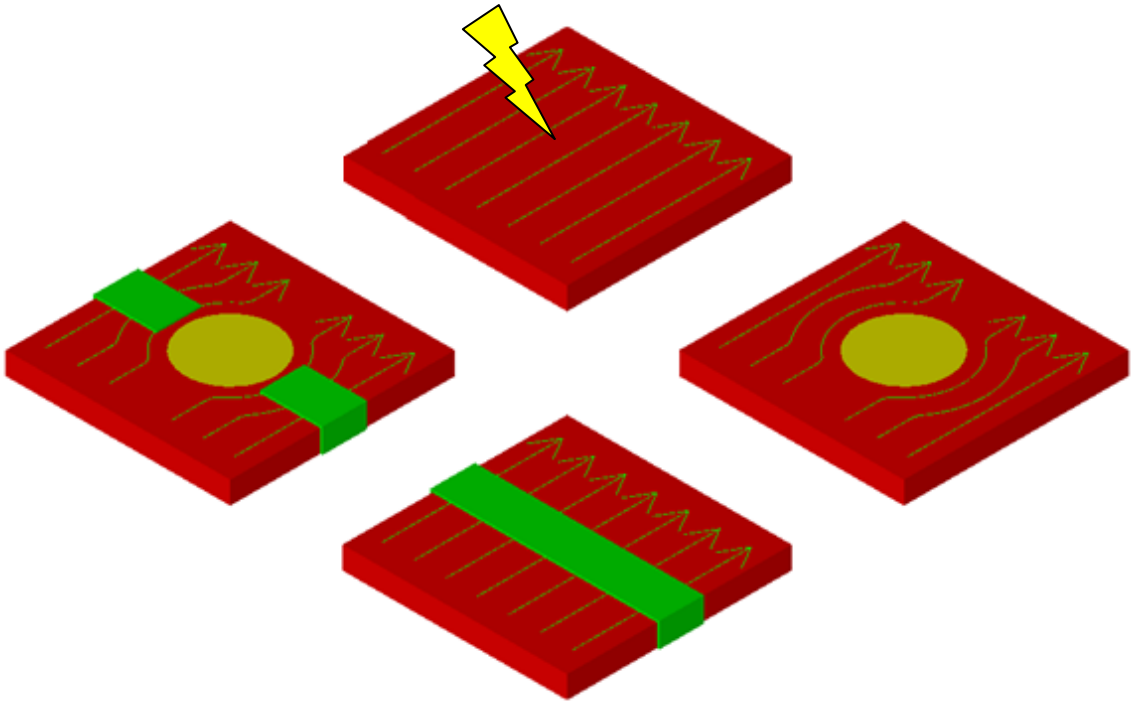

Figure 1 The hotspot creation process. First a photon is absorbed by the nanowire, then the hotspot expels the current, the current density becomes too high and a resistive segment is formed.

This is also the reason why nanowires are used. In bigger materials or bulk, the absorption of a photon wouldn't cause a resistive segment and therefore no voltage change. The photon wouldn't be measured, which is why nanowires are used instead. After the creation of the resistive piece, the nanowire starts to cool down and eventually becomes superconducting again.

The increase in voltage can be measured indirectly because the SNSPD is in parallel with a load resistance of ~ 50 Ω. (see figure 2). When the wire is superconducting, all current will flow through the wire. When (part of) the wire becomes normal, the resistance in the wire (which is about three orders of magnitude larger than the load resistance) causes most of the current to flow through the Z_0. The voltage change over the load can then be measured.

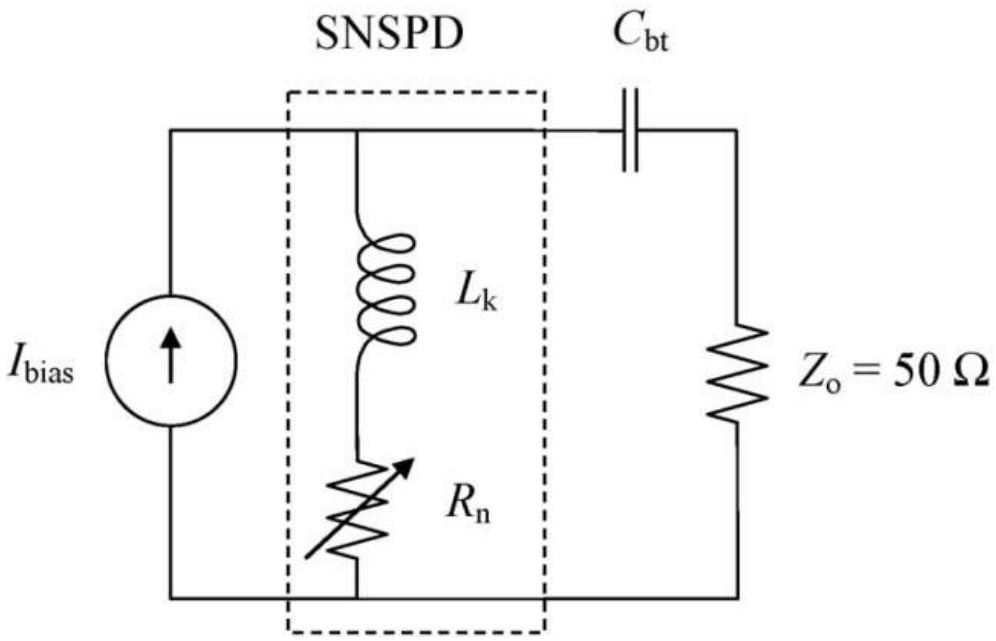

Figure 2 The equivalent of the electrical circuit with the SNSPD simulated as a inductance and resistance in series. [3]

2.3 Noise sources

Electrical measurements are followed by electro-optical measurements for the best devices. 'Best devices' refers to the detectors with a reasonable critical current that will give a measurable voltage pulse after amplification. This is typically above 10 μA.

The goal of electro-optical characterization is to measure the electrical pulses produced by photon absorption. There are two sources of possible errors in these measurements. The first one is electrical noise. Electrical noise is created by the instruments used during the experiments but also instruments connected to the same ground even if they are not used in the experiments. The connections between the devices and the cables are also a source of electrical noise. This noise is measured when everything is connected but the wire is not biased yet. The electrical noise can be eliminated by setting a trigger level on the oscilloscope or the counter. The second source of error is represented by dark counts, which are pulses not related to the optical signal of interest. Basically, dark counts are false measures in the experiment, which are not caused by the absorption of light that is directed on the wire. Measuring the dark count is required to eliminate those "false counts" from the real counts, originated by the light shined on the detector. It is suggested that these dark counts can be created by the unbinding of vortex-antivortex pairs in the wire, causing a resistance although this has not yet been proven [1,2]. Another cause of dark count can be a hotspot creation due to the absorption of background radiation.

2.4 Goal and approach

In order to know the properties and quality of the nanowires the IV curve of a nanowire is analyzed. To obtain the I-V curve of the wires, voltage biasing is used. When the bias voltage of the circuit is changed, the voltage drop over Z_0 is measured using a DC multimeter. This voltage drop is then transferred into the current through Z_0 (Z_0 is known) to get a curve like shown in Figure 3 below.

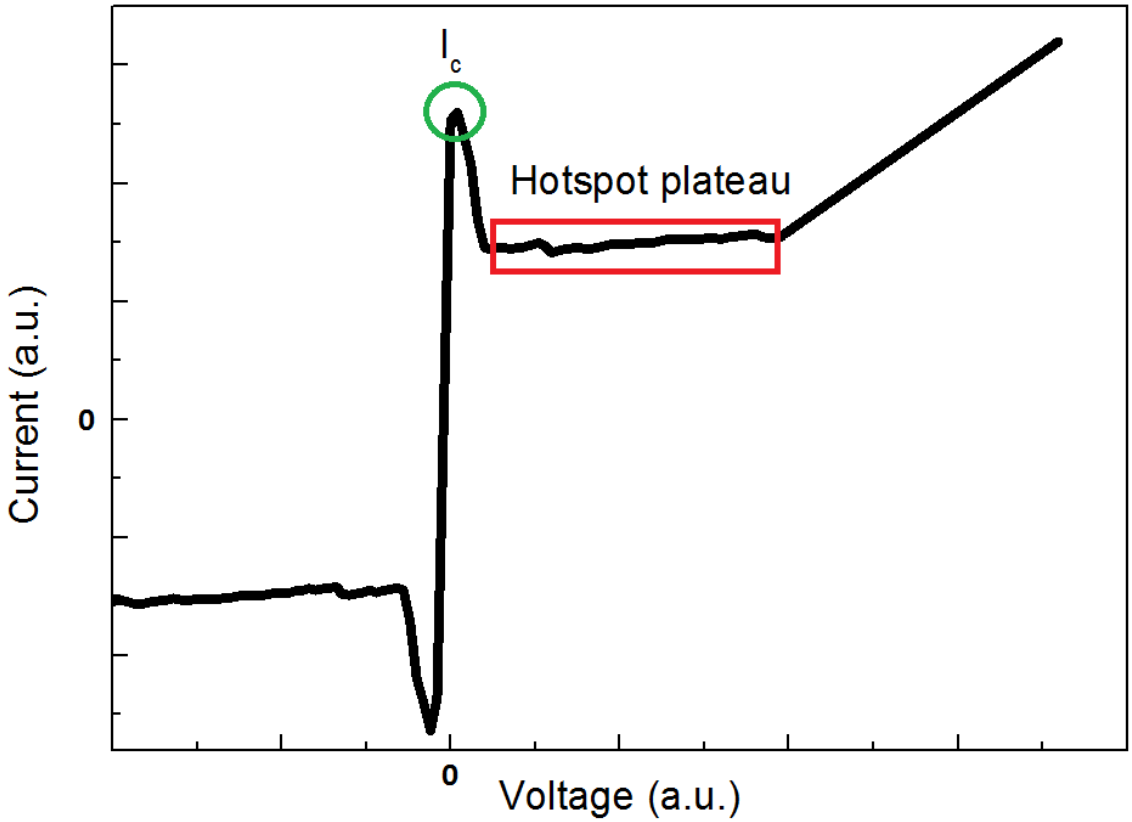

Figure 3 An example of an IV curve. Ic is the critical current of the superconducting wire and the hotspot plateau is where the hotspot is growing along the nanowire.

Since the wire is superconducting for $I < I_c$, the slope of the linear part of the graph around zero can be used to calculate the external circuit resistance, which is basically due to bias resistance in the circuit. The maximum current is the critical current of the nanowire. After this, the current density through the wire is too large and a segment of the wire has to become resistive. Now the voltage is still increased, but the current doesn't increase. This is called the hotspot plateau. Here, the hotspot is expanding along the wire due to the increase in the resistance of the wire. After the complete wire has become resistive, it will be a simple resistive wire and will obey ohm's law (equation (1)).

$$V = R \cdot I \tag{1}$$

Here, V is the voltage, R the resistance of the wire and I the current through the wire. From this, the resistance of the nanowire at low temperature can be calculated.

The goal of this project is to get information about the TU/e grown nanowire single photon detectors. How uniform is the NbN film? How variable is the thickness and width of the nanowires? Why are some devices not working? Are the wires broken, is there a bad connection with the contact pads,..? And of course: Do these nanowires work as single photon detectors, and why (not)? In this project, we will try to answer these questions.

3 Modeling method

Computer simulations can be used to get a better understanding of the behavior and functionality of SNSPDs. Specifically, the electrical and thermal response of the superconducting nanowires after a photon is absorbed. This can be done by using an electrical model of the circuit and the nanowire and a thermal model of the nanowire, respectively. However, since the electrical properties at a time change the thermal properties correspondingly, it's better to combine these models and make one electro-thermal model [3]. The simulation calculates the heat flow along the wire in time. This way the recovery time of the wire can be found. This is the time needed for the wire to become superconducting again after a hotspot is created. However, if the wire is heated up too much, it cannot cool down fast enough and the current will cause even more heat. Now, the whole wire will become resistive. This effect is called latching.

This has been proposed by [3] and the simulation has been used in this report is written by a PhD student, Saeedeh Jahanmirinejad. Simulations are done with Matlab.

3.1 Thermal model

The SNSPD is approximated as a one dimensional structure. This is because the nanowires are very thin (with thickness d ≈ 4-5 nm) and narrow (with width $w \approx$ 80-150 nm) compared to the length ($l \approx 17$ μm) for this experiment. At time zero, a Δx segment (25 nm) of the wire is considered to become normal (namely resistive) due to photon absorption. The current density J through the wire and temperature T of the wire is assumed to be uniform in one segment. This T is solved using the following equation:

$$J^2\rho + \kappa\frac{\partial^2 T}{\partial x^2} - \frac{\alpha}{d}(T - T_{sub}) = \frac{\partial cT}{\partial t} \tag{2}$$

Here, ρ is the electrical resistivity of the wire, which is zero when the wire is in superconducting state and non-zero when the wire is in normal state. κ is the thermal conductivity of NbN, α is the thermal boundary conductivity between NbN and the GaAs substrate, T_{sub} is the substrate temperature, T is the temperature of one segment and c is the specific heat per unit volume of NbN. In (2), the first term is the heat generated due to the Joule heating, the second term is the dissipated heat along the wire due to thermal conduction and the third term is the heat dissipated into the substrate. The term on the right hand side is the rate of change in the local energy density.

The values for the variables ρ, κ, α and c depend on the temperature of the wire and its state (normal or superconducting). In order to calculate these variables, the critical current at temperature T has to be calculated. This can be done with the equation below.

$$I_c(T) = I_c(0) \cdot \left(1 - \left(\frac{T}{T_c}\right)^2\right)^2 \tag{3}$$

Here, $I_c(T)$ is the critical current at temperature T, $I_c(0)$ is the critical temperature at absolute zero and T_c is the critical temperature. Because I_c cannot be measured at $T = 0$ K, but only at a finite T, it can be derived from (3) using $I_c(T = 5\,K)$ and $T_c = 11\,K$ measured on another film grown in the same batch. From this, it follows that:

$$I_c\,(0) = \frac{I_c(T)}{\left(1 - \left(\frac{T}{T_c}\right)^2\right)^2} \tag{4}$$

These values can then be used in this simulation.

The electrical resistivity ρ can be calculated from

$$\rho = R \cdot \frac{A}{L} = R \cdot \frac{w \cdot d}{L} \tag{5}$$

R is the resistance of the wires and measured during the experiment and width *(w)*, length *(L)* and thickness (*d)* are found in the devices measured by scanning electron microscopy and ellipsometer, respectively. The value of ρ can then be used in the formula below [1] to calculate α.

$$I_{hs} = \sqrt{2} \cdot \sqrt{\frac{\alpha \cdot w^2 \cdot d \cdot (T_c - T_{sub})}{\rho}} \tag{6}$$

$$\Rightarrow \quad \alpha = \frac{I_{hs}^2 \cdot \rho}{2 \cdot w^2 \cdot d \cdot (T_c - T_{sub})}$$

Where I_{hs} is the hotspot current, extracted from the IV curves (as in figure 3) of the experiments. I_{hs} is proportional to the width and thickness of the nanowire and proportional to $1/\rho$ as a higher electrical resistivity will decrease the current.

The last parameter is κ. It can be calculated by using the Wiedemann-Franz law:

$$\kappa = \frac{L \cdot T}{\rho} \tag{7}$$

Where $L = 2.45 \cdot 10^{-8}$ $\mathrm{W\Omega/K^2}$ is the Lorenz number. With ρ calculated before, the temperature dependent normal state conductivity κ_n can be calculated. The superconducting state thermal conductivity κ_s can be calculated from $\kappa_s/\kappa_n = T_c/T$ [3], because in (7), *L* and ρ are constant.

3.2 Electrical model

The electrical circuit of the SNSPD is modeled as shown below in Fig 2. The SNSPD is seen as an inductor L_k , representing the kinetic inductance of the superconducting nanowire, which is the total kinetic energy of the cooper pairs that acts as a series inductance. The kinetic inductance is in series with a resistance R_n which is the variable resistance of the normal segment of the nanowire which is zero while the wire is in superconducting state.

The C_{bt} is the capacitor located in the bias T in the experiments and represents the DC block towards the RF amplifiers and the oscilloscope. Z_0 is a 50 Ω load resistance, which is used to indirectly measure the voltage pulse created by the hotspot. The current through the nanowire can be solved by [3]

$$C_{bt}\left(\frac{d^2 L_k I}{dt^2} + \frac{d(IR_n)}{dt} + Z_0 \frac{dI}{dt}\right) = I_{bias} - I \tag{8}$$

Here, R_n is temperature dependant and determined by the thermal model.

4 Experimental set-up

4.1 Electrical characterization set-up: Micro-probe station

The sample is first glued to a sample holder with a cryogenic glue (CMR 7031 GE varnish), with a good thermal conductivity. Good thermal conductivity is required to thermalize the devices to the cryostat temperature. This way, the heat can also more easily be conducted away from the sample to the holder. Since the GaAs substrate of the sample is not a very good heat conductor, a clamp is placed on the top side of the sample to improve the heat transfer between the sample and the holder.

Then, the sample (on a holder) is placed inside the cryostat. An aluminum plate with an optical window is placed a few centimeters above the sample. The plate is for filtering the lower energy photons (with higher wavelengths). This way, there is less dark count in the experiments. The plate also has aluminum curtains on one side which hang over and next to the probe to improve for better blocking of the thermal background radiation. The top of the cryostat is then closed with a plate containing an optical window.

The probe is connected from room temperature to the cryostat through a tube and manipulated at room temperature. There is also the possibility to place a second probe in this setup, but it is not necessary for this experiment. There is also a line for creating a vacuum in the cryostat and one for the helium.

4.1.1 The probe

The microprobe is an RF probe from GGB industries, Inc [4]. There are three fingers located in a row. The outer ones are used as ground and the middle one is the bias. The probe can be moved in the x-, y- and z-direction.

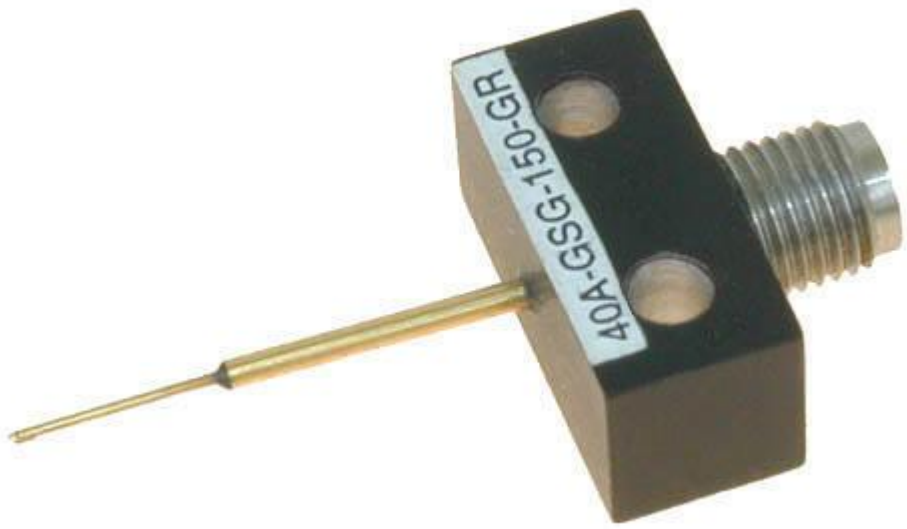

Figure 4 An example of a probe of the same type used during the experiments. [4]

4.2 Optical characterization set-up

In order to see the three fingers of the probe and the sample in more detail, a ccd camera is used. A lamp has to be focused on the sample to get a clear view with the camera. To do this, the optical arm below is used.

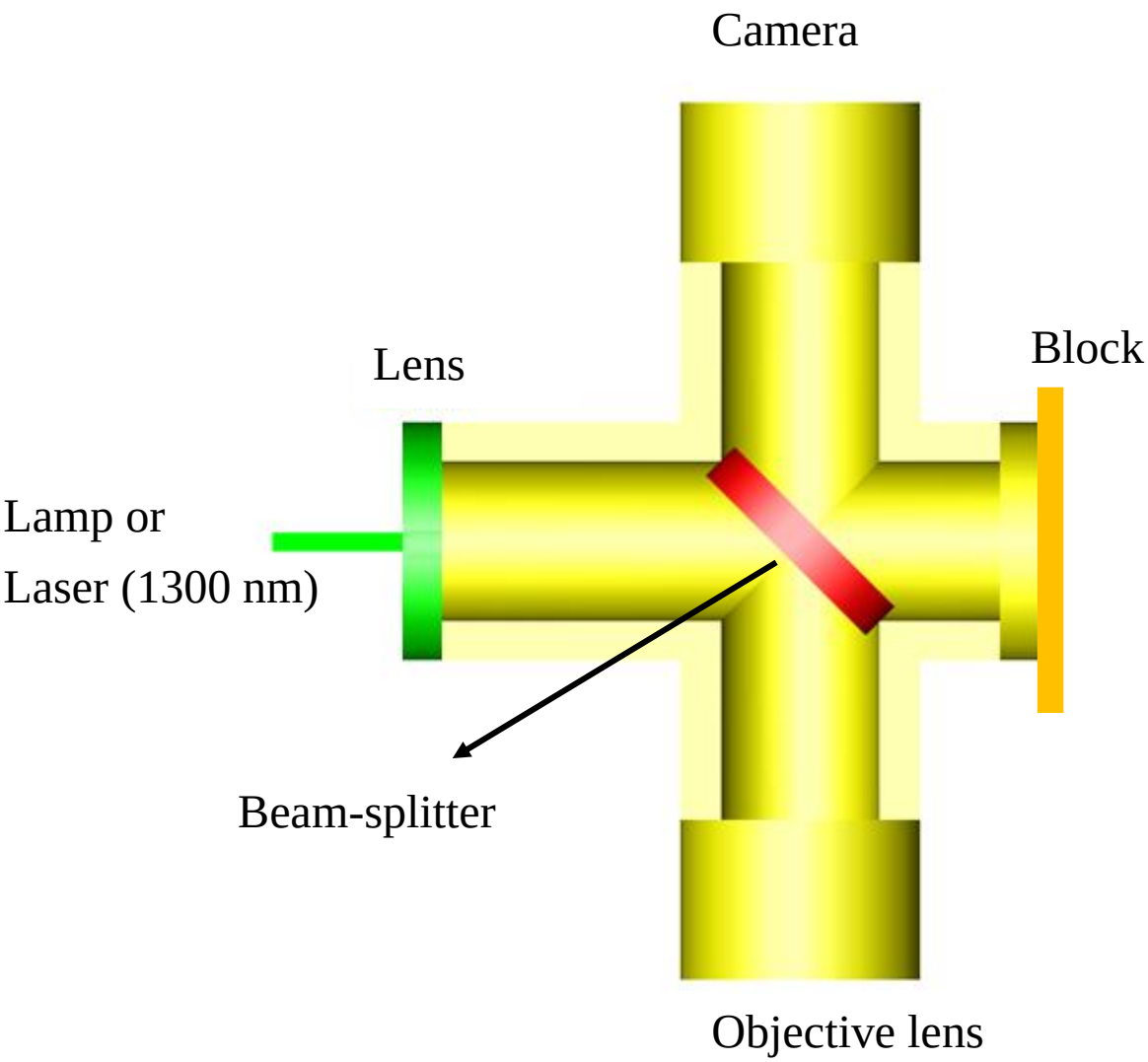

Figure 5 The optical part of the setup.

In this setup, a beam splitter is used to point the light and camera simultaneously at the sample. The lens is used to create a parallel light beam, which can be checked at the right side (block). Then, the beam splitter is placed at 45^0, so the light goes parallel through the center of the vertical cylinders between the mirror system and the camera. Finally, the mirror system of the objective is used to focus the light on the sample inside the cryostat.

On the right side, there is a block to block the light (when a laser is used on the left) for safety reasons. It is however possible to put the sensor of a power meter here in order to measure the transmitted power during the optical measurements as a reference measurement. With some calibration measurements, it is then possible to calculate the

actual (reflected) power on the sample by measuring the transmission power (since the ratio between transmitted and reflected light is constant).

4.3 Electronics

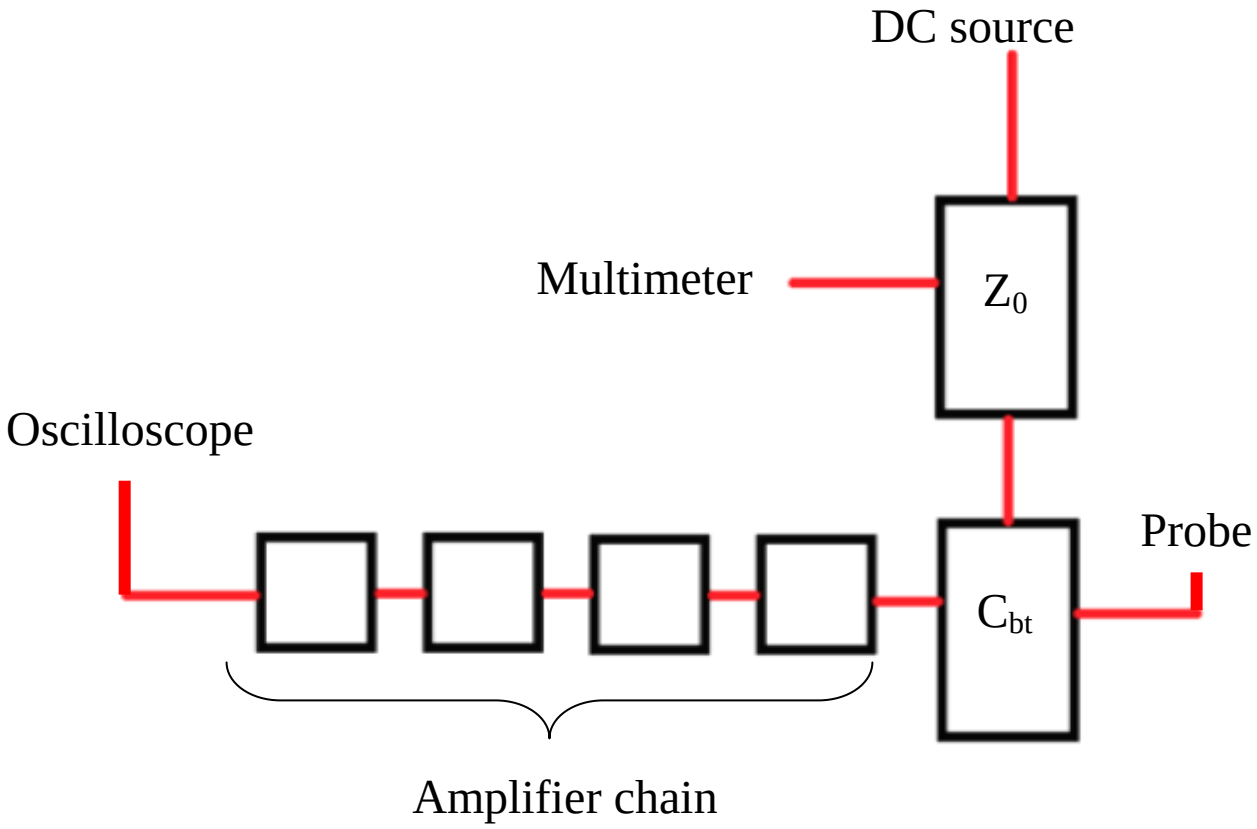

Figure 6 The electronics used in the experiments. The bias T is the block connecting the probe, resistance and amplifier chain.

A schematic view of the electrical circuit is shown above. Here, a Yokogawa 7651 DC source is used to bias the circuit. When the probe touches down on the sample on the contact pads, the circuit is closed and a current can flow through the probe and thus the nanowire. The multimeter (a Agilent 34970A) can be used to measure the resistance of the wire, the voltage over the wire or the substrate temperature. Z_0 is the load resistance. The bias T in the circuit contains a capacitor which works as a dc block towards the amplifiers and the oscilloscope. The amplifiers are required to get a measurable signal on the oscilloscope.

4.4 Sample Design

The samples that will be measured and analyzed in this experiment contain single nanowires with different lengths and widths and are grown by DC magnetron sputtering technique on a GaAs substrate. The wires are made of NbN and are connected to gold (Au) contact pads with a wider section of NbN, which is optically not active due to its larger dimensions. The probe can be contacted to the Au pads for electrical contact.

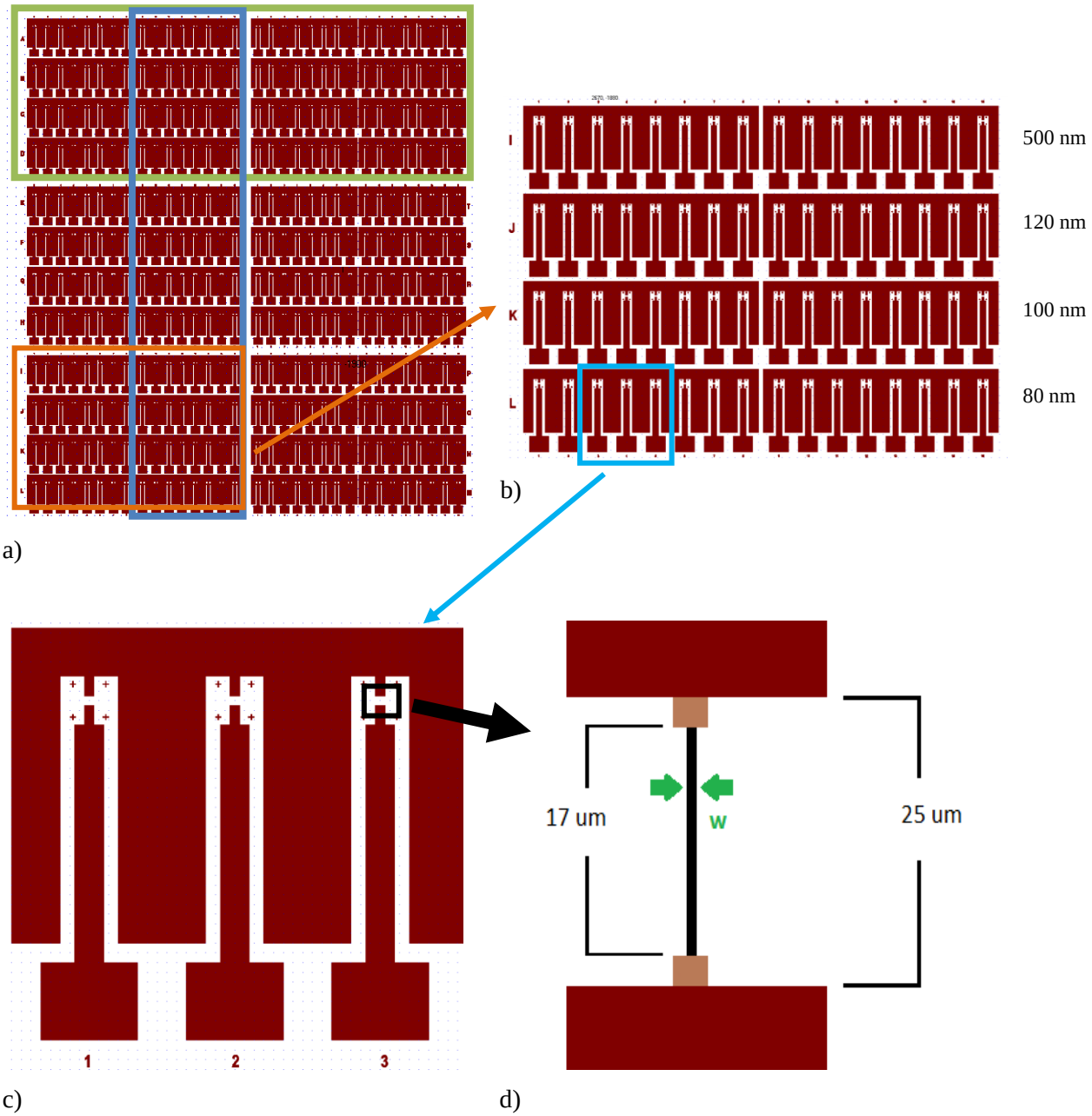

Figure 7 The top left image a) shows the top view of one complete sample. The blue block contains the wires with variable length, the green block contains the wires that are not measured in this report. b) shows one block with 16 devices in a row and every row a different width for the nanowires. Every device is labeled with a letter and a number. c) Three devices in more detail. The E shape is the ground, the part with the number below is the bias. The nanowire is located between the ground and the bias as shown in more detail in d).

The image above shows the top view and shows the structure of a sample. As seen in the drawing, one 'device' consists of a ground and a bias (outer and inner Au pads,

respectively) and a nanowire. The grounds of 8 sequential devices are connected, and then a new set of devices starts. All devices can be identified by a letter and a number from 1 through 16, giving a total of 24 x 16 = 384 devices on one whole chip. The width of the nanowires in one row is the same, but changes per row. This is shown on the image above. The length of the wires is expected to be 17 μm, except for the wires in the blue block (see figure 8.a). These wires vary in length between 1 and 10 μm. (Those wires are not analyzed in the frame of this report). The devices in the green block are not measured in this report because they are cleaved from the sample. This is because the sample holder in the cryostat is not large enough for the whole sample. Also, some devices on the left or right side of the remaining sample are lost during the measurements because they are located below the clamp used to thermalize the sample.

In this experiment there are four samples measured, all of which have the same design and structure described above. The difference is that they were grown in different batches, meaning the thickness and growth temperature of the NbN layer are varied for different batches. Also the uniformity and niobium vs. nitrogen concentrations might vary between the samples from different batches. Even though there is no observable change between the flows of different batches, there are always variations due environmental influence. For that reason, two samples grown in different batches with the same parameters (namely GaAs C155 and C157) are processed. Also, one sample is grown at a lower temperature to see whether this will have a measurable influence on the performance and quality of the nanowires. Below, there is a table containing the samples with the thicknesses of their NbN layer, critical temperature T_c and growth temperature of the NbN layer.

Sample name	Thickness (nm)	T_c (K)	Growth temperature (° C)
GaAs C152-1t	5.94	10.1	410
GaAs C155-1t	5.64	11.7	450
GaAs C156-1t	4.90	11.2	450
GaAs C157-1t	5.51	11.7	450

Table 1 The samples measured in this experiment with their thicknesses, critical temperature and growth temperature.

The critical temperatures in the table above are extracted from the R-T measurements performed by Döndü Sahin. The results for these measurements are shown in figure 8. These are typical curves for NbN films. As seen, T_c is thickness and growth temperature (T_g) dependent. With a higher T_g, due to improvement of film uniformity, T_c is higher. This is also valid for thicker films, which I related to the proximity effect [17].

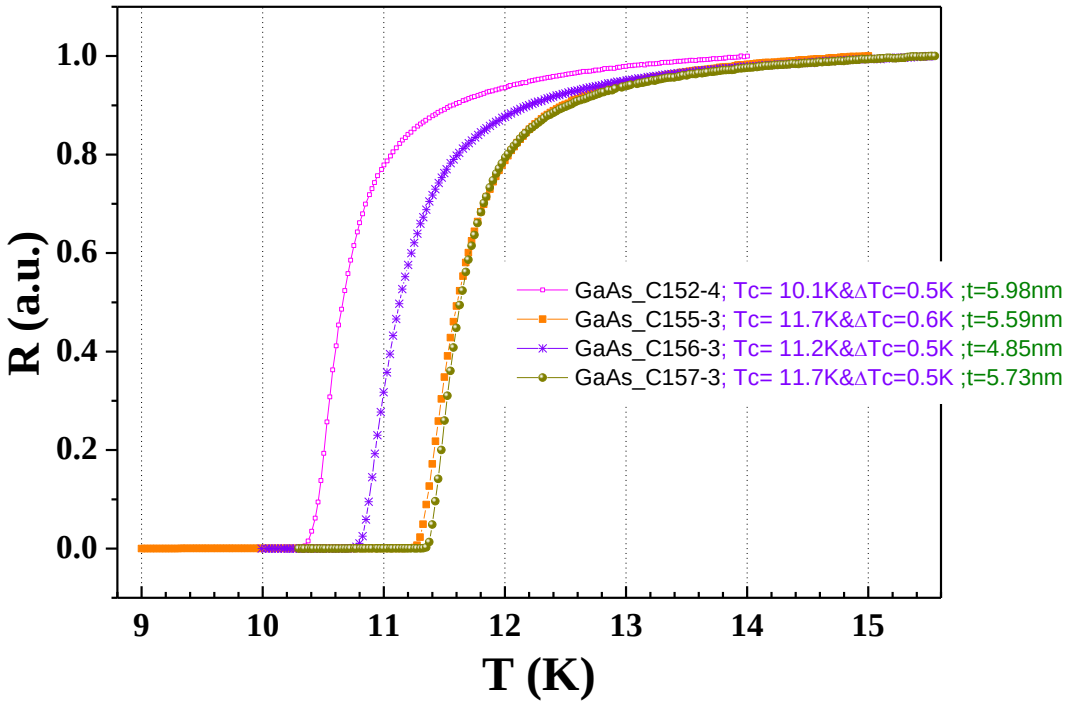

Figure 8 The normalized R-T curves for samples from the same batches as the ones used in this project.

5 Results and discussion

The main motivation of this work is to improve the yield and detection efficiency of the superconducting single photon detectors. Therefore, a total of four samples is measured to characterize the nanowires and to get information on the quality and performance of the different samples with different thicknesses and growth temperatures. This is done by measuring several properties of the samples like the room temperature resistance R_n, a characteristic IV curve and an extended IV curve. From these curves, the low temperature resistance R_{LT} and the critical current I_c are extracted and used to look at the quality of the NbN films and the nanowires themselves. There are also scanning electron microscopy (SEM) measurements performed to get some images and measure the dimensions of the nanowires. With these SEM images, the real width and length of the nanowires can also be measured. Last, some optical measurements are performed to see if the devices are working as photon detectors.

5.1 IV curves

The IV curves of the nanowires already give an idea on the quality of the nanowire and its connections with the bias and ground. They also show if the device is short or open. An example of a good (Figure 9) and a bad (Figure 10) wire is shown in the image below.

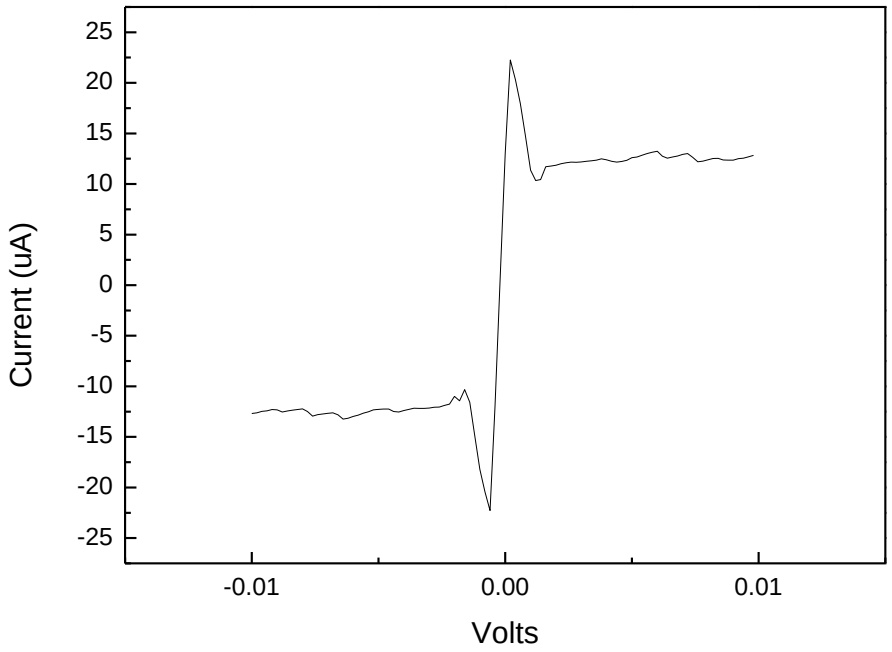

Figure 9 Example of a good functioning nanowire with a clear critical current value and a clear hotspot plateau.

The IV curve above shows the expected behavior, with an expected Ohm resistance of the bias resistor (measured when nanowire is superconducting), a clear I_c and a nearly horizontal hotspot plateau.

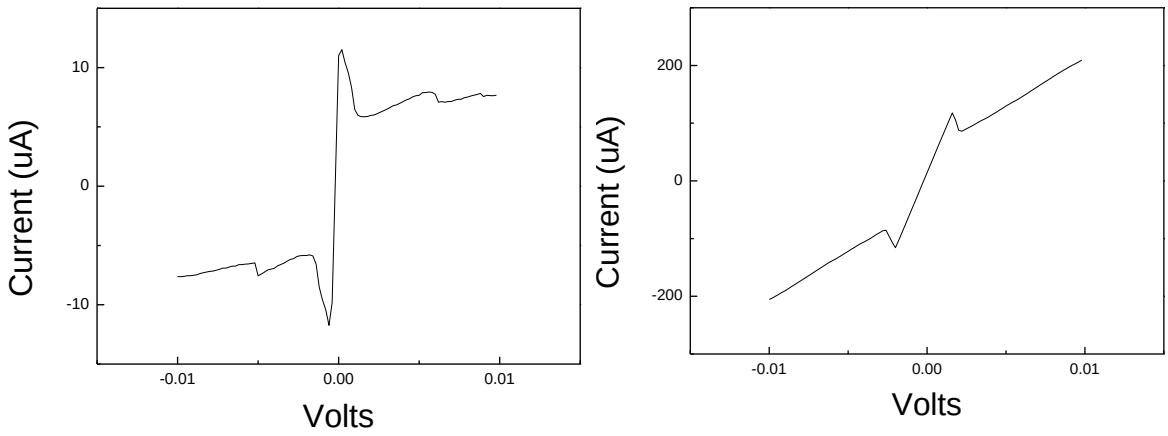

Figure 10 Examples of nanowires which are not functioning properly. The one on the left has a unstable hotspot plateau and the one on the right has no hotspot plateau at all.

The image above shows IV curves of devices that are not functioning properly. There is almost no hotspot plateau.

The IV curves of all wires with the same width from one sample as shown in Figure 11 are combined to give an idea about the variation of the curve namely the uniformity of the devices on one sample. The curves for the other widths of this sample and of the other samples can be found in appendix 9.1.

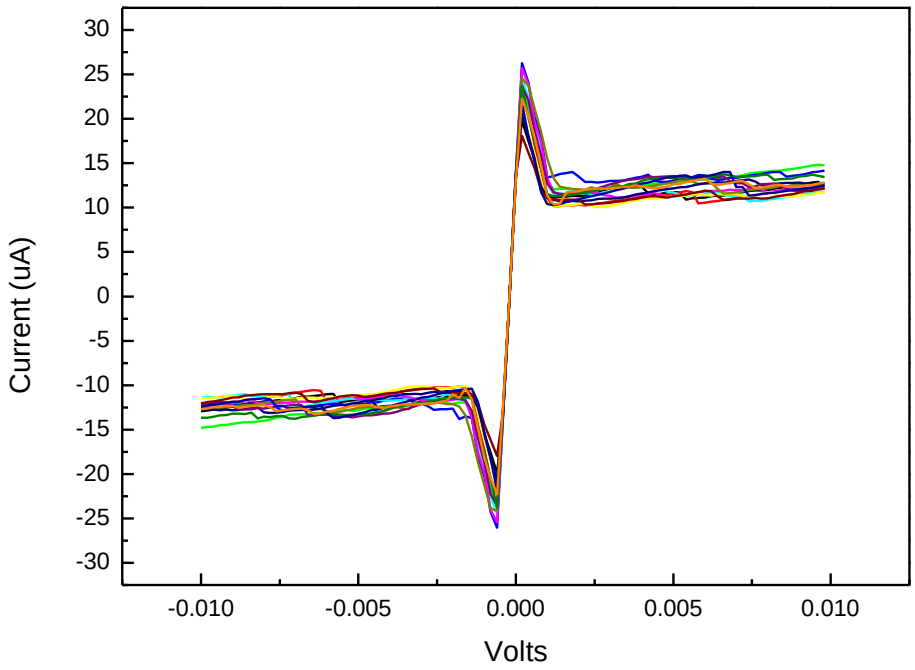

Figure 11 The IV curves of the 120 nm wide nanowires from the GaAs C156-1t sample.

In the graph above, the IV curves of the 120 nm wide nanowires from the GaAs C156-1t sample are plotted together. It is clear that there is some variation in the critical current and the hotspot current, but that the values are within a range of approximately 5 μA from

the average number of 22 μA.. This will be analyzed further in the statistical analysis in this report.

During the measurements, it became clear that some wires did not give any response. This was related to the processing after SEM analysis and the reasons were either the wires were broken or not properly connected. There were also devices that were short. In most of these cases the shortage was visible with the camera. It showed a direct connection of the Au-contacts (the bias and the ground). An example is shown in the image below.

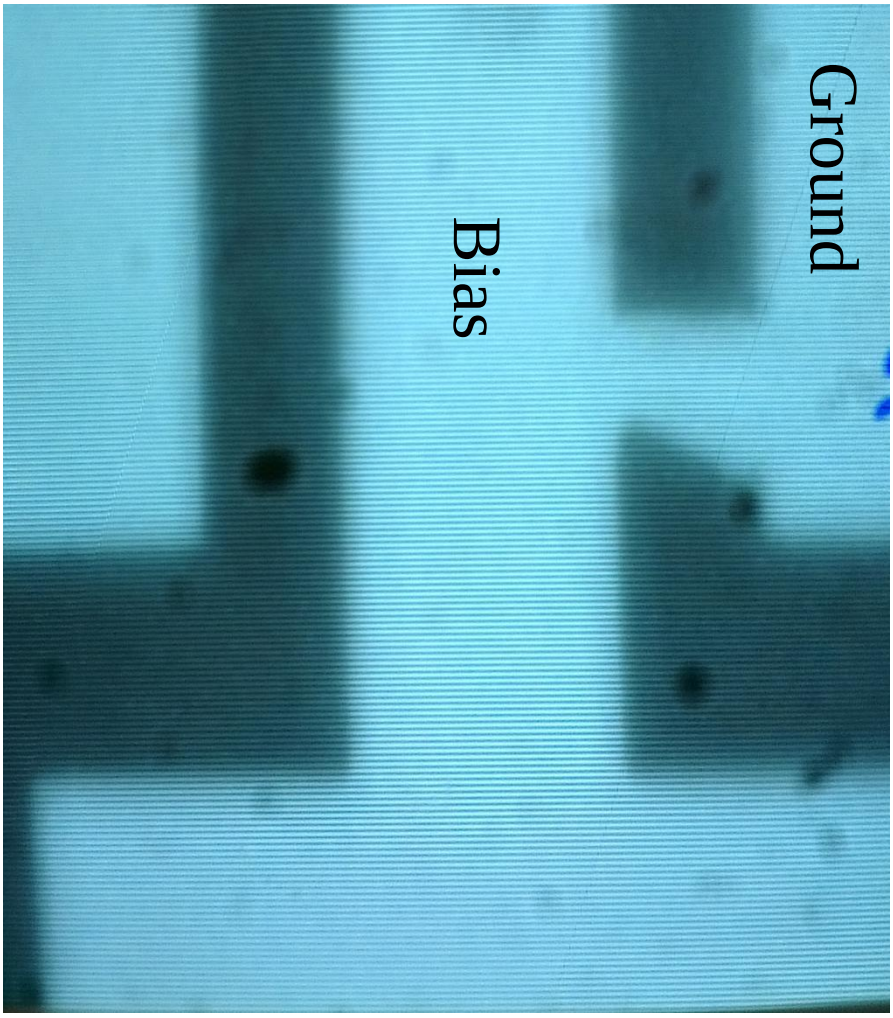

Figure 12 The bias and the ground are clearly connected creating a short in the circuit.

These proces defects are caused by lithography processes. In order to get an idea on the number of working wires, the yield of every sample is calculated. This is the percentage of the wires measured and that is actually working.

Sample name	Yield (%)
GaAs C152-1t	80
GaAs C155-1t	44
GaAs C156-1t	80
GaAs C157-1t	97

Table 2 The samples with their respective yields.

It is clear that the GaAs C155-1t sample has a very low yield. The left half of the sample has almost no nanowires functioning. Less than 10 wires could be measured and even these wires have relatively low critical currents compared to the wires on the right side of the sample. On the right side of the sample, there are actually 80% of the devices working properly. The reason for that is that during the processing, EBL dose was not enough to write the patterns.

The most likely explanation for this is that something went wrong during processing. This is checked with SEM.

5.2 SEM measurements

The SEM measurements are performed by Döndü Sahin. These measurements are done to check the real width of the nanowires. The widths given before are the desired widths of the nanowires, but not the real widths of the wires on the samples. Also, these measurements are done to see what the problem is for the 'open' nanowires and the nanowires with extreme critical current and resistance values. Since those are the first processing batches on NbN in the clean room in TU/e. Thus, SEM analysis is going to give an understanding of what went wrong during the processing so it can be avoided in the future.

5.2.1 Actual widths

The actual widths of the nanowires are measured on devices that have critical currents around the average of the nanowires with the same width. Then, a few of these nanowires are measured per width per sample. The measured values are then averaged and this average is used as the actual width of all those nanowires on one sample. The actual values found for the width of the nanowires is shown in the table below. These values are obtained by measuring the width of several nanowires with SEM and average them.

Sample name	Type 80 nm (nm)	Type 100 nm (nm)	Type 120 nm (nm)	Type 500 nm (nm)
GaAs C152-1t	89.5±5	99±5	109±5	402.5±20
GaAs C155-1t	98±5	115±5	133±5	338±20
GaAs C156-1t	103±5	118±5	136±5	403±20
GaAs C157-1t	107±5	112±5	131±5	380±20

Table 3 The samples with the actual widths of the nanowires for every type of wire.

For the scope of this report, and to avoid confusion, the desired widths (or type) are used in all other graphs and explanations unless otherwise stated. However, the real widths of the nanowires are used in the calculations of the variables and parameters.

5.2.2 Device defects

The SEM images from the devices that are not working show several different reasons for why the devices are broken. In some cases, the nanowire is broken. In others, there is a small gap or opening between the end of the nanowires and the contact pads. In the case of the GaAs C155-1t sample, where there are a lot of devices not working, the SEM images show that in most cases there are no (or only partial) nanowires between the contacts. The measurements also show some pollution, particles on the surface touching the nanowire. The examples of all these defects can be seen in the images below.

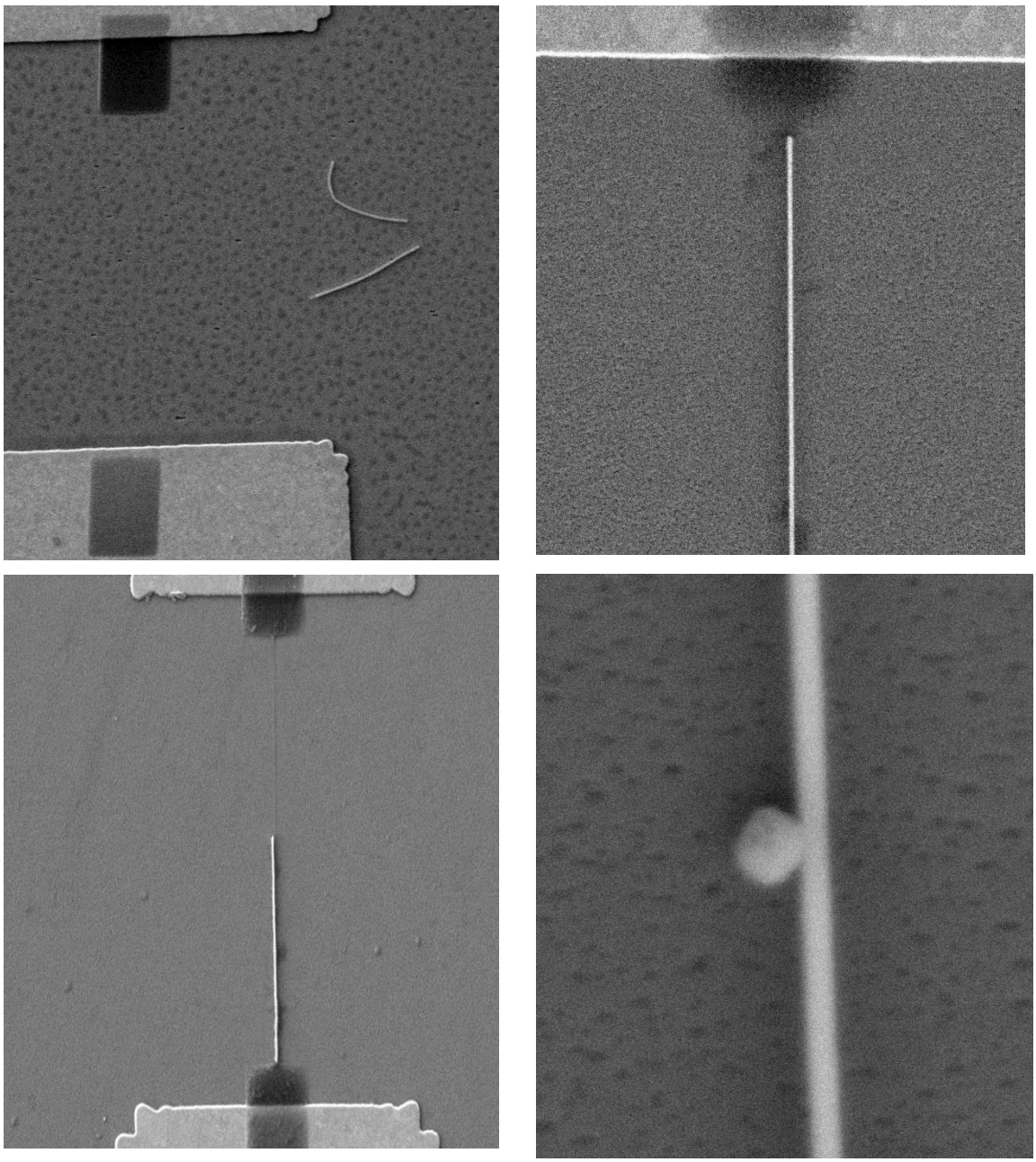

Figure 13 The top left image shows a nanowire that is broken and moved. The top right side shows a bad connection between the nanowire and the contact pad. The bottom left image shows only a partial wire, with a piece missing. The bottom right image shows an undesired particle touching the nanowire, creating a constriction in the nanowire.

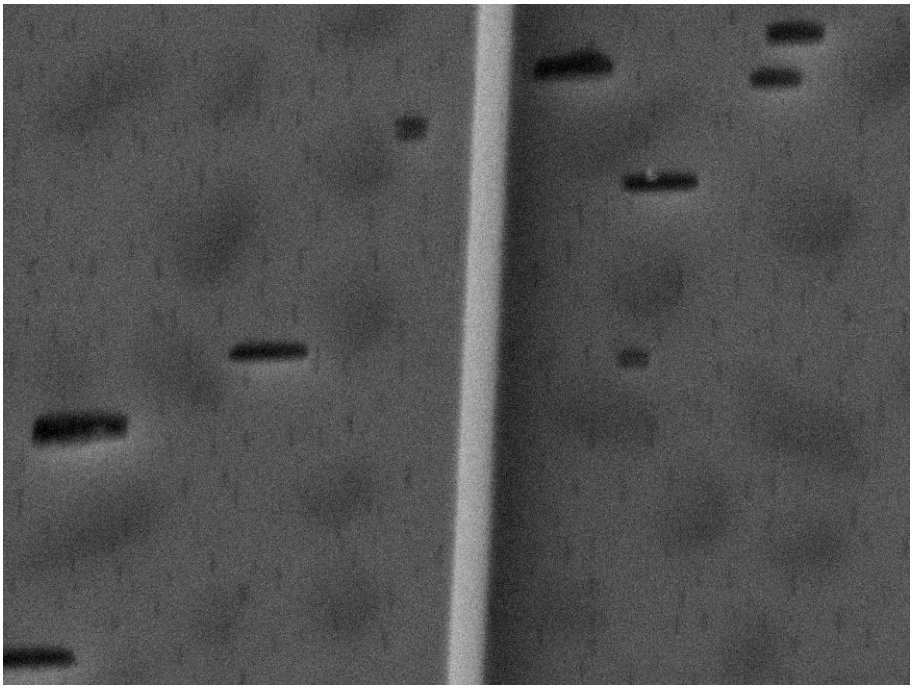

Figure 14 The black stripes are some surface irregularities.

As can be seen in the last image above, some samples suffer from a roughness on the surface of the GaAs layer. This surface isn't measured, only the nanowires are, but the roughness may also be underneath the nanowires. When the NbN layer was grown on this surface, the roughness may have influenced the growth of the NbN and thus the thickness and uniformity of the nanowire in the end.

5.3 Statistical analysis

Using a statistical analysis, it is possible to get information about the uniformity and the quality of the NbN film and the nanowires. In this report, a few different methods will be used and compared in an attempt to get more information about the devices.

5.3.1 Critical current statistics

The critical current is dependent on the width and the thickness of the nanowires. The statistics is performed by counting the number of devices that have a value in a range of 1μA, because this is the average variation of the I_c measured several times on one device. Only the nanowires with the same width from the same sample can be directly compared. An example of this is shown in the image below.

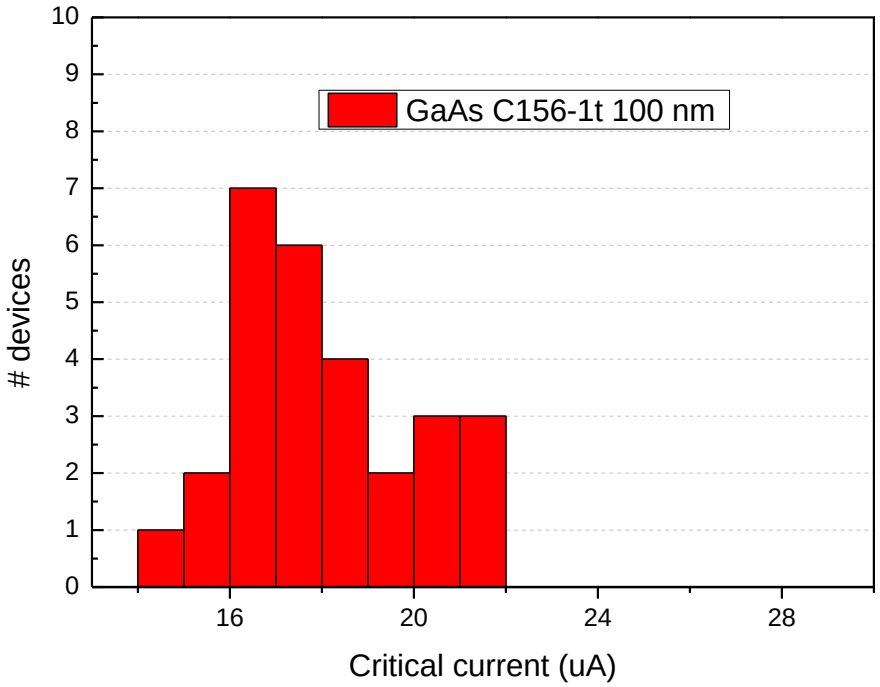

Figure 15 The critical current statistics for the 100 nm wide nanowires of GaAs C156-1t.

As can be seen in the graph above, the number of devices used in one analysis is very low. This is because there are only a few devices (between 10 and 50) with the same width in one sample that could be measured and were actually working. This is why there was looked for other parameters that are independent of the width and thickness of the nanowires. That way, all wires within one sample can be compared and also, the samples can be compared with each other.

The average and the standard deviation for every width are calculated for every sample. Also the percentage of the standard deviation against the average is calculated to get an idea about the size of the distribution. The results are found in table 4.

I_c

Sample name	Width (nm) →	80	100	120	500
GaAs C152-1t	Average I_c (uA)	12.28	14.44	18.89	46.69
	σ_I (uA)	2.12	2.73	2.10	5.35
	σ_I / I_c (%)	17.30	18.89	11.13	11.45
GaAs C155-1t	Average I_c (uA)	16.38	18.58	25.21	49.83
	σ_I (uA)	2.13	3.37	1.02	5.96
	σ_I / I_c (%)	13.01	18.14	4.06	11.96
GaAs C156-1t	Average I_c (uA)	14.09	18.23	21.74	48.90
	σ_I (uA)	2.64	3.20	2.35	3.11
	σ_I / I_c (%)	18.76	17.55	10.80	6.37
GaAs C157-1t	Average I_c (uA)	15.66	17.42	21.20	45.61
	σ_I (uA)	2.02	1.90	1.44	4.08
	σ_I / I_c (%)	12.93	10.9	6.79	8.95

Table 4 The average, standard deviation and percentage per width per sample.

5.3.2 I_cR_n statistics

One way to eliminate the width and thickness dependence is using the I_cR_n method [5]. In this method, the critical current (I_c) of a nanowire is multiplied by the room temperature resistance (R_n) of the nanowire.

$$I_c = J_c \cdot A = J_c \cdot w \cdot d \tag{9}$$

$$R_n = \rho \cdot \frac{L}{A} = \rho \cdot \frac{L}{w \cdot d} \tag{10}$$

Then, by multiplying (7) and (8), it follows that:

$$I_c \cdot R_n = J_c \cdot \rho \cdot L \tag{11}$$

which is independent of the width and thickness of the nanowires. Note that this method only eliminates the variation in the whole width of the nanowire, not local constrictions. If there is a small local constriction in a nanowire, like shown below, this will determine the critical current of the nanowire and this method will not correct for that (see figure 16). This local constriction causes the critical current to decrease much more than the resistance. This is because the critical current is only dependent on the smallest constriction of the nanowire, while the resistance is also dependent on its length.

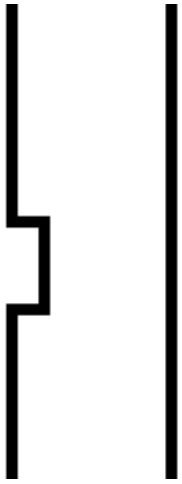

Figure 16 Schematics of a local constriction in a nanowire.

The values of I_cR_n are then normalized per sample by the maximum value of I_cR_n in the same sample. Then, the devices within a range of 0.025 are counted. The graphs for the four different samples separately can be found in appendix 9.2. The graphs for the comparison between the samples are shown below.

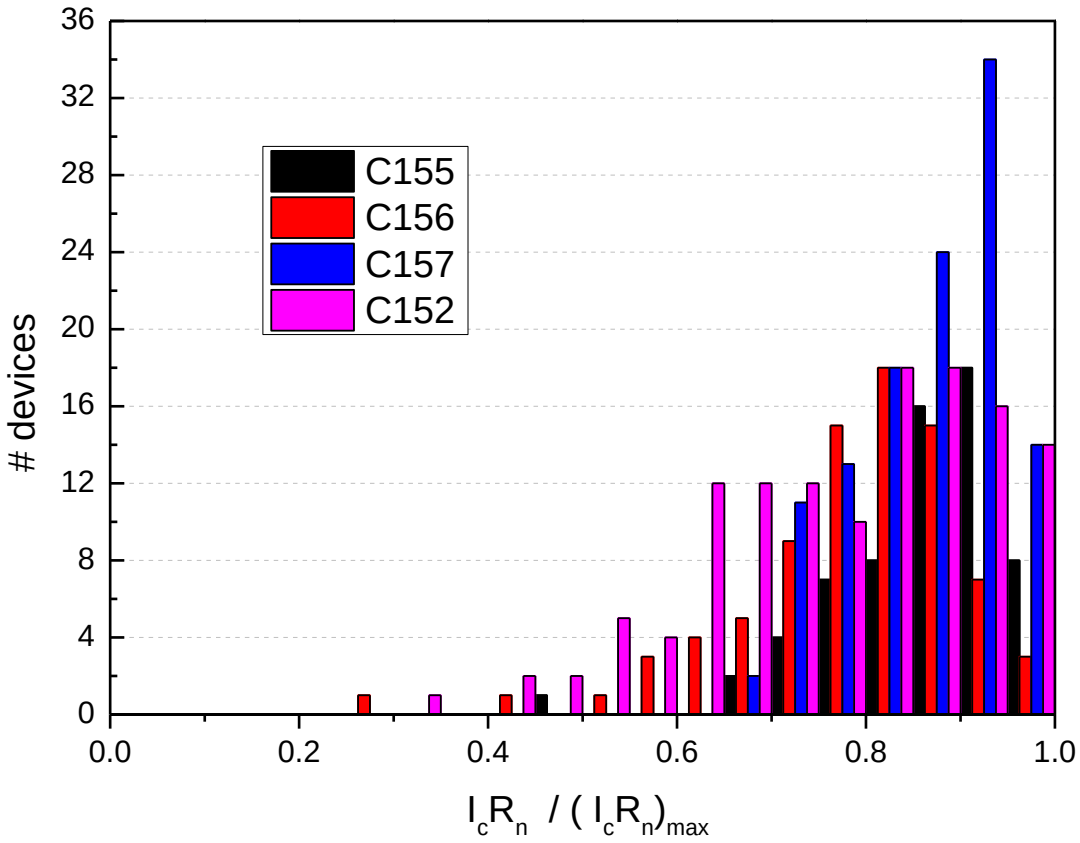

Figure 17 The statistics of all four samples plotted together in one graph. Every sample has a different color to show the differences in distribution between the samples.

In the graph above, the number of devices per range is counted for all samples. Then the values for all samples are plotted together. Note that also here, it is the distribution of the nanowires that matters, not the height of the graphs that is related to number of devices, because some samples have more working wires than others. From these I_cR_n values, the

average, standard deviation and percentage is also calculated. The results are shown in the table 5 below.

$I_cR_n/(I_cR_n)_{max}$

Sample name	Nominal Width (nm) →	80	100	120	500	Total
GaAs C152-1t	Average	0.729	0.738	0.882	0.713	0.780
	Standard deviation	0.188	0.149	0.134	0.139	0.144
	(%)	16.22	20.23	15.14	19.48	18.47
GaAs C155-1t	Average	0.784	0.815	0.919	0.849	0.862
	Standard deviation	0.078	0.123	0.038	0.069	0.095
	(%)	9.95	15.14	4.13	8.19	11.04
GaAs C156-1t	Average	0.697	0.803	0.826	0.838	0.785
	Standard deviation	0.125	0.125	0.082	0.032	0.120
	(%)	18.0	15.55	9.94	3.76	15.35
GaAs C157-1t	Average	0.842	0.862	0.889	0.871	0.866
	Standard deviation	0.084	0.080	0.044	0.066	0.076
	(%)	9.98	9.30	5.00	7.54	8.75

Table 5 The average, standard deviation and percentage of IcRn/(IcRn)max of every type of nanowire per sample and the total for one sample.

The percentages in table 5 show the relative standard deviation compared to the average. This shows for example that the nanowires with a width of 108 ± 10 nm in the GaAs C152-1t sample are quite widespread (20%). This means that they have a lot of physical (local or uniformity) constrictions. For the GaAs C157-1t 122 ± 15 nm nanowires, they are only 5.00% apart, so there are much less constrictions in the nanowires.

The values of all samples can also be summed up. This is done in the graph below.

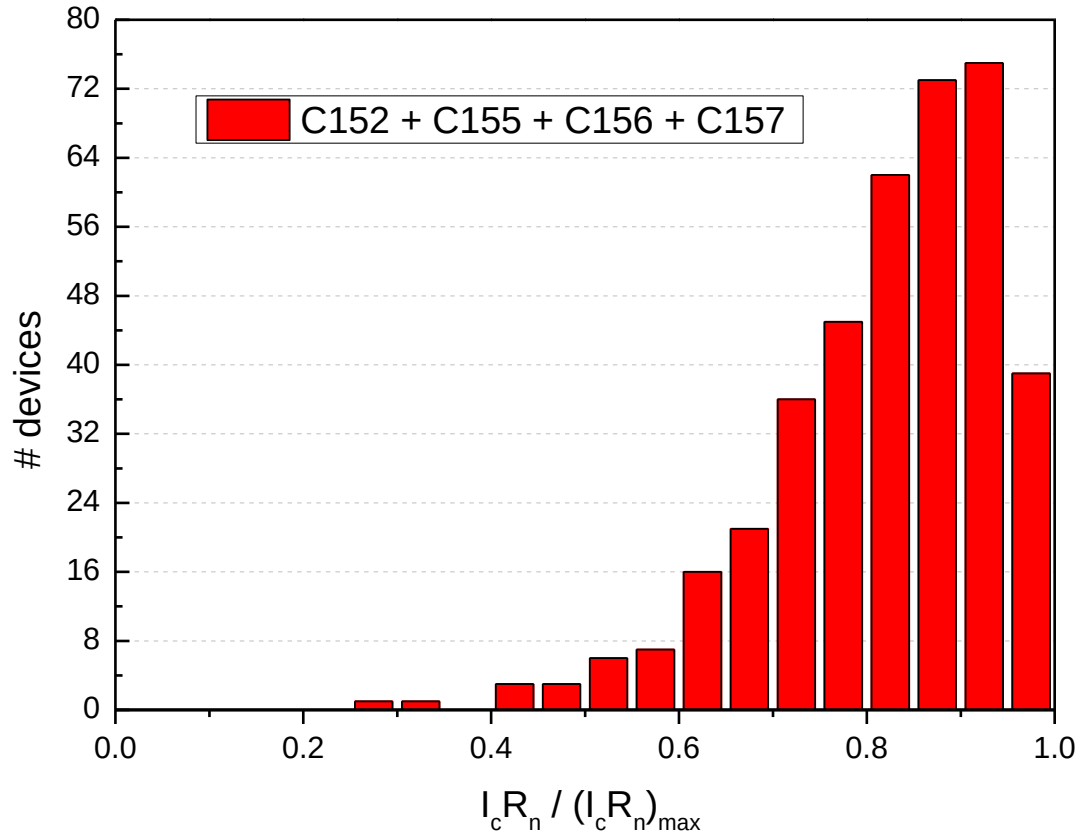

Figure 18 The number of devices/ nanowires in one range are summed up from all samples. This shows the distribution of all nanowires together.

In figure 18, the maximum reaches a value of 76, and a more continuous distribution is shown.

5.3.3 J_c analysis

Another way to compare and analyze the nanowires, is by calculating the critical current density J_c. It can be calculated by

$$J_c = \frac{I_c}{d \cdot w} \tag{12}$$

with I_c the critical current of the nanowire, d the thickness and w the width of the nanowire. The value for the thickness d of the nanowire is measured with the ellipsometer by Döndü Sahin. The width used in this calculation is the average width of the nanowires from one sample with the same width. This is measured using the SEM. The I_c is extracted from the IV curves as explained before. The results for the four samples separately are shown in appendix 9.3.

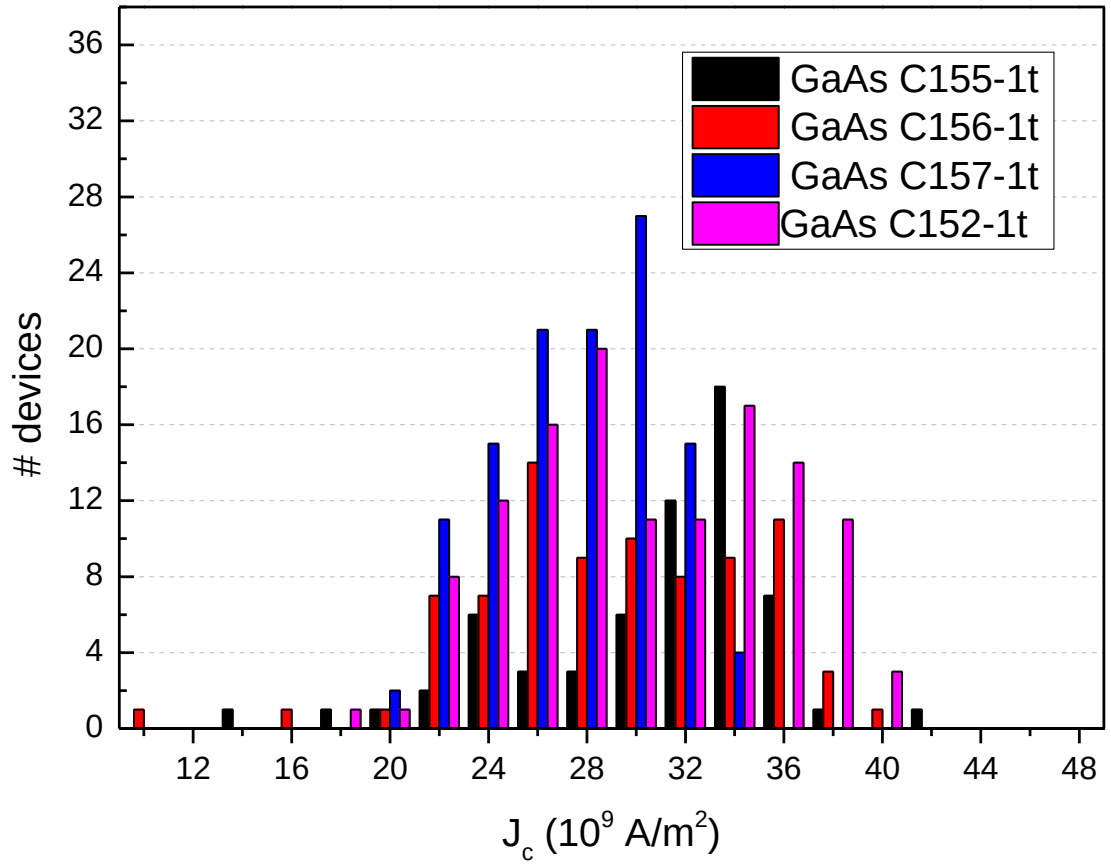

Figure 19 The J_c statistics plotted in one graph for the four different samples.

In figure 19, again the distribution over J_c is more important than the height of the curve, which only represents the number of devices. The average of the different type of nanowires and the total average of one sample are represented in table 6. The standard deviation of each average and the percentage of the standard deviation compared to the average is calculated.

J_c

Sample name	Width (nm) →	80	100	120	500	Total
GaAs C152-1t	Average J_c (10^9 A/m^2)	23.23	24.56	29.35	19.53	24.25
	σ_{J_c} (10^9 A/m^2)	4.00	4.64	3.29	2.24	5.16
	σ_{J_c} / J_c (%)	17.20	18.89	11.20	11.45	21.29
GaAs C155-1t	Average J_c (10^9 A/m^2)	29.63	28.65	33.60	23.25	30.87
	σ_{J_c} (10^9 A/m^2)	3.86	5.20	1.37	2.78	5.10
	σ_{J_c} / J_c (%)	13.02	18.14	4.06	11.96	16.51
GaAs C156-1t	Average J_c (10^9 A/m^2)	27.92	31.52	32.63	24.76	29.11
	σ_{J_c} (10^9 A/m^2)	5.24	5.53	3.52	1.58	5.45
	σ_{J_c} / J_c (%)	18.76	17.55	10.80	6.37	18.71
GaAs C157-1t	Average J_c (10^9 A/m^2)	26.56	28.23	29.38	24.49	27.52
	σ_{J_c} (10^9 A/m^2)	3.43	3.08	1.99	2.19	3.36
	σ_{J_c} / J_c (%)	12.93	10.90	6.79	8.95	12.21

Table 6 The critical current density J_c statistics. The average, standard deviation and percentage is calculated for all different widths from every sample. Also, the total for one sample is calculated.

In table 6, there is a general trend showing that the standard deviation compared to the average is decreasing as the width of the nanowires increases. This can be explained by the fact that the smaller nanowires are more sensitive to local constriction on the surface and sides of the nanowire. Also, processing is more difficult for smaller nanowires.

5.4 Comparing I_c, J_c and I_cR_n methods

Ideally, the J_c method and the I_cR_n method should give the same standard deviation compared to the average ($\frac{average}{standard\ deviation}$). The table containing all the data can be found in appendix 9.4.

From this table, it is clear that there is no change in the percentage when comparing the I_c and J_c values. This is obvious, as J_c is proportional to I_c. When the percentages for J_c are compared to those of I_cR_n, it is clear that in most cases the I_cR_n method has a slightly smaller deviation. This would mean that the values of the different nanowires are closer together. This could be explained by the fact that with the I_cR_n method, the width and thickness of a nanowire is eliminated by the actual width and thickness of the nanowire. This is because the R_n is actually measured separately for every nanowire, which means that the width and thickness in that formula are exactly the same as those is the formula for I_c. In the J_c method however, the width and thickness are calculated by taking the average of several measured real widths from one type of nanowire. So the width used in the calculations for J_c are the average widths for all the wires of that same type, not the real widths. Also, the thickness is measured using an ellipsometer. This gives one value

for the whole sample, while there is still the possibility for some variation in the thickness along the sample. So this value is also not exact for all the wires. This results in some more variation in the values for J_c.

When looking at table 7 in appendix 9.4, it is clear that samples C155 and C157 have a higher J_c. They also have more uniform J_c and I_cR_n. This may be explained by the thicker NbN film. This way, the non uniformity of the surface of the NbN nanowires does not influence the current as much as in thinner nanowires. Sample C156 has a higher current density than C152, but is less uniform than samples C155 and C157, because the nanowires are thinner. The I_cR_n method reduces only slightly the standard deviation compared to the J_c. This can be either because the defects are local as shown in figure 16. Another possibility is that there are defects that affect only J_c and not R_n. The J_c values are calculated with an average width for all nanowires of the same type on one sample. The real width of several of these wires was measured with SEM. In the I_cR_n method however, the R_n is measured for each nanowire separately. This way, the width is really eliminated from the equation where in J_c this is not possible because the used width is an average value.

5.5 RRR analysis

Residual Resistivity Ratio or RRR is a value used to indicate the purity or impurity of a metal. A pure metal generally has a value larger than one, while dirty metals, like semiconductors usually have a value smaller than one. In most cases, it is calculated by

$$RRR = \frac{R_{300}}{R_{20}} \tag{13}$$

Where $R_{300}$is the resistance at 300 K and R_{20} the resistance at 20 K. In more general terms, it is the resistance at room temperature divided by the low temperature resistivity. In this experiment, the resistance is measured at the temperatures 293 ± 5 K and 12 ± 5 K. Also in this case, a statistical analysis is performed.

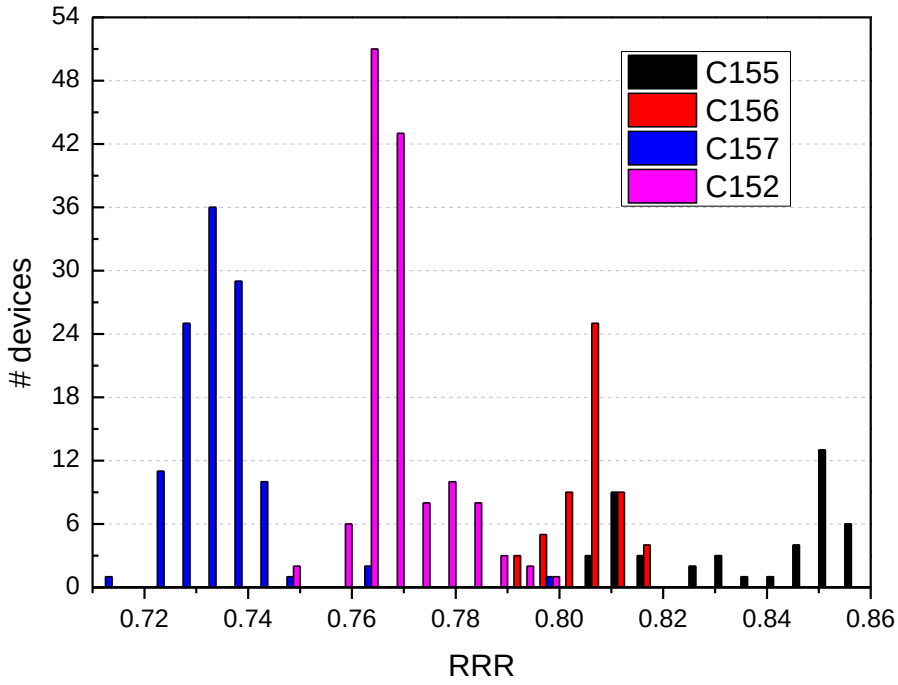

Figure 20 The RRR of every sample plotted against the number of devices.

In figure 20, the RRR value is plotted against the number of devices. It is clear that, although the distribution is similar, the averages per sample are not. This can be explained by the difference in thickness of the different samples. When the thickness of the sample increases the resistance becomes less sensitive for interface effects on the surface of the nanowires. It is expected that the RRR increases slowly to one as the thickness of the sample increases. A graph of the RRR value against the thickness of the nanowires is shown in figure 21.

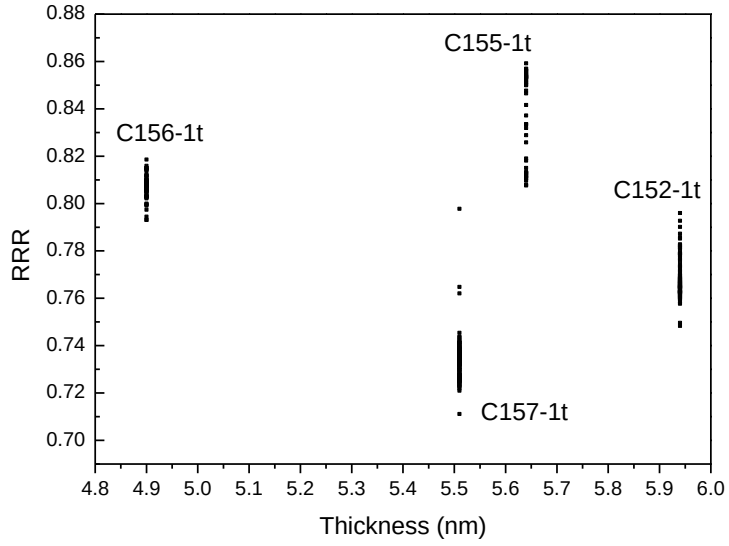

Figure 21 The RRR values from each sample against the thickness of the sample.

In this figure, it is clear that the expected slight increase from left to right is not valid. The change between the GaAs C156-1t and C155-1t sample is the expected behavior. But the GaAs C157-1t is completely different and doesn't coincide with the expectations. The reason for this could be that there are more impurities in the nanowires or different concentrations of Nitrogen. It could also be related to local temperature variations.

5.6 Optical analysis

The electrical response of the nanowires under illumination with a xxx nm laser is studied. The first measurements showed no response of the nanowires. They are performed on 370 ± 35 nm nanowires from the GaAs C157-1t sample. The first problem is the noise created by the connection and the electronics. Specifically, the amplifiers cause a lot of noise. This noise could be greatly reduced (> ten times) by improving the connections between the amplifiers and between amplifier and probe/oscilloscope. However the measurements showed no difference between the laser off and laser on measurements.

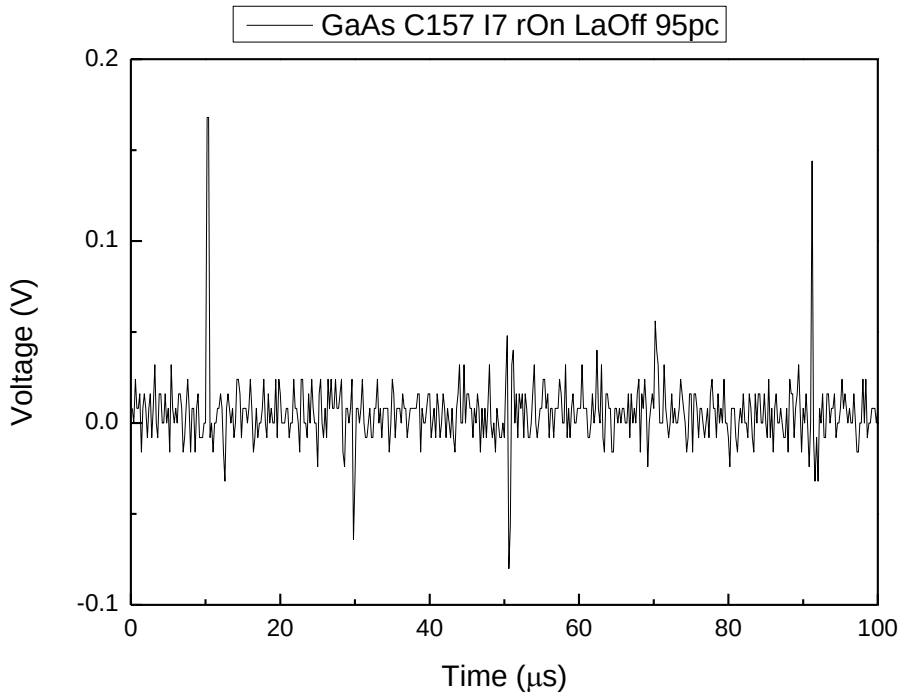

Figure 22 Oscilloscope trace of the voltage measured from a laser off (left) and laser on (right) 370 ± 35 nm wide nanowire.

In figure 22, there seem to be periodic pulses with a period of about 20 μs. An explanation for this has been suggested by Dauler [6], which explains that the periodic pulses are caused by the discharging of the capacitor.

Another problem with these 370 ± 35 nm nanowires is that they are latching. This can be supported by the elctro-thermal simulation described in section (3) and choosing the parameters close to the values of the nanowire, which are experimentally obtained. An optical response from these nanowires was also not expected to occur.

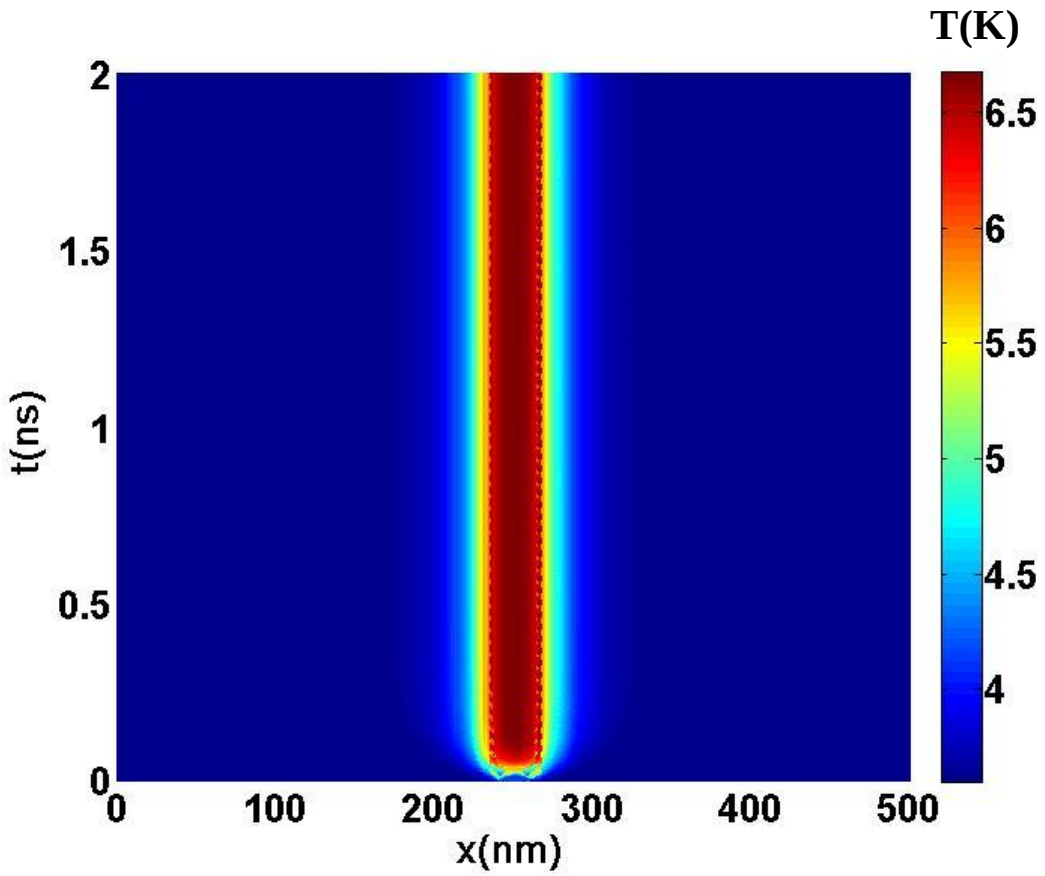

Figure 23 Temperature of a 400 nm wide nanowire. The simulation confirms that this type of nanowire should be latching.

In figure 23, The y-axis represents the time and the x-axis represents the direction along the nanowire. The simulation sees the nanowire as a one dimensional object, so the hotspot is assumed to be along a segment of the wire. The x-axis only shows a total of 500 nm because this is the nanowire length used in the simulation. The real length of the nanowire is still used to calculate the variables (like the kinetic inductance). The simulation runs only through 500 nm because this decreases the simulation time (compared to 17 μm) and if the hotspot is 500 nm in length on the wire, it will be latching anyway.

5.6.1 80 nm nanowires

The simulation is looped through small changes of the critical temperature, critical current at temperature *T*, the low temperature resistance, the hotspot current and the substrate temperature. This is done in an attempt to find the boundary conditions where the nanowire switches between the functioning state as a single photon detector and the latching state. Last, there are some simulations performed when adding a series inductance to the nanowire.

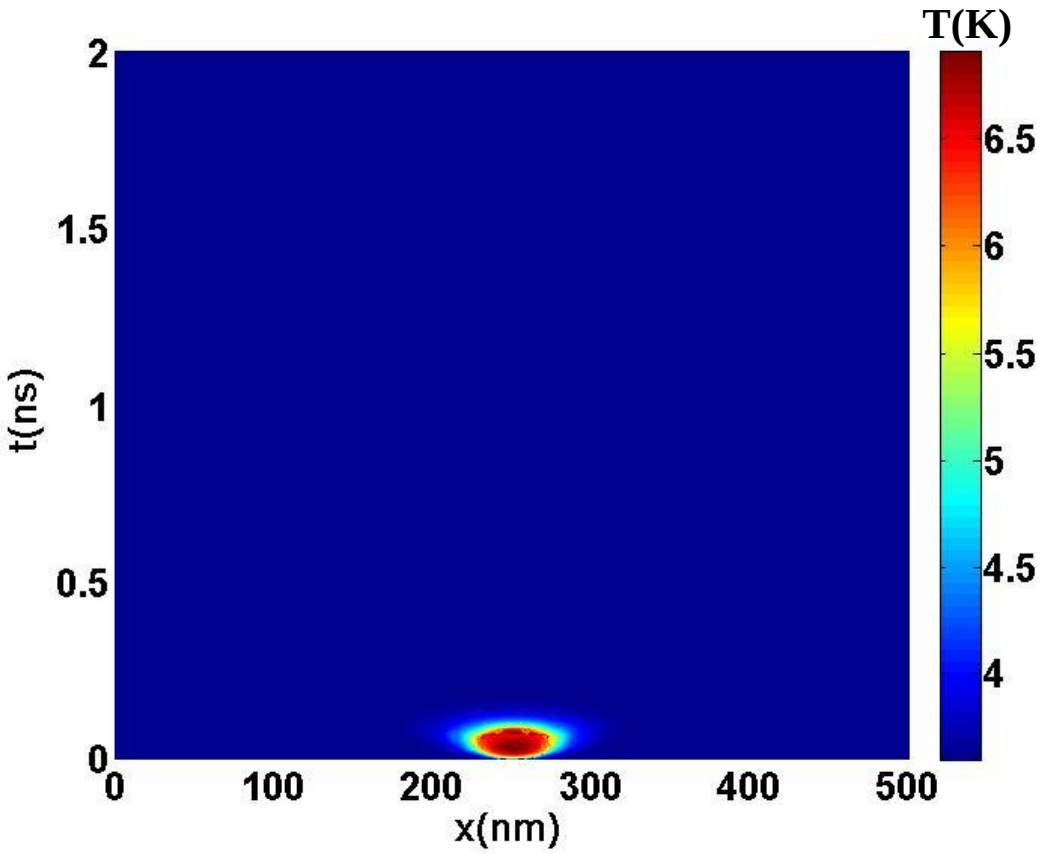

Figure 24The thermal simulation image of an 80 nm nanowire with the hotspot size against time.

In figure 24 is a thermal image visible from the simulation of an 80 nm nanowire. In this scenario, the wire shows no latching behavior.

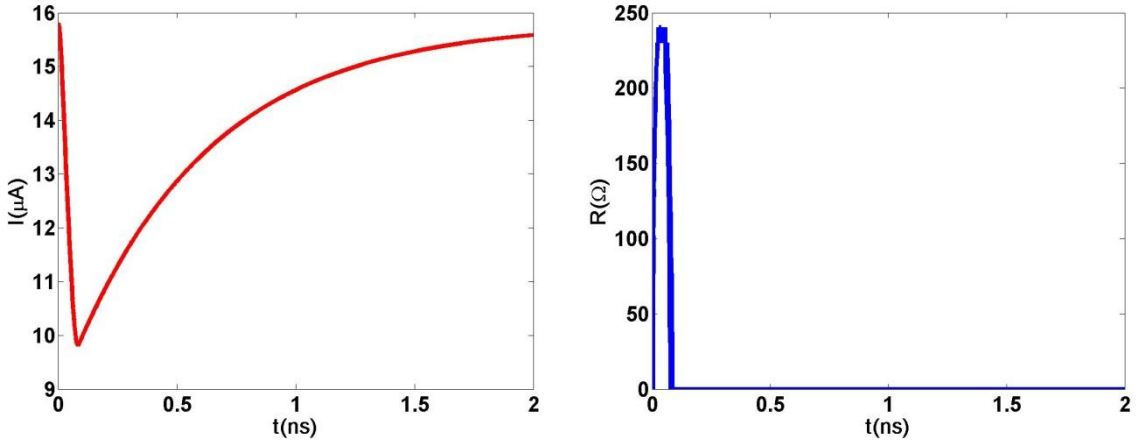

Figure 25 The current through the nanowire against time graph and the resistance of the nanowire against time.

In figure 25, the current through the nanowire and the resistance of the nanowire against time are plotted. From the resistance plot, the time that *I* is recovering back to its superconducting value gives an idea about the pulse width when it is measured with the oscilloscope. Also, both graphs in figure 25 show that the nanowire recovers completely within two nanoseconds and becomes superconducting again. There is no latching behavior in this.

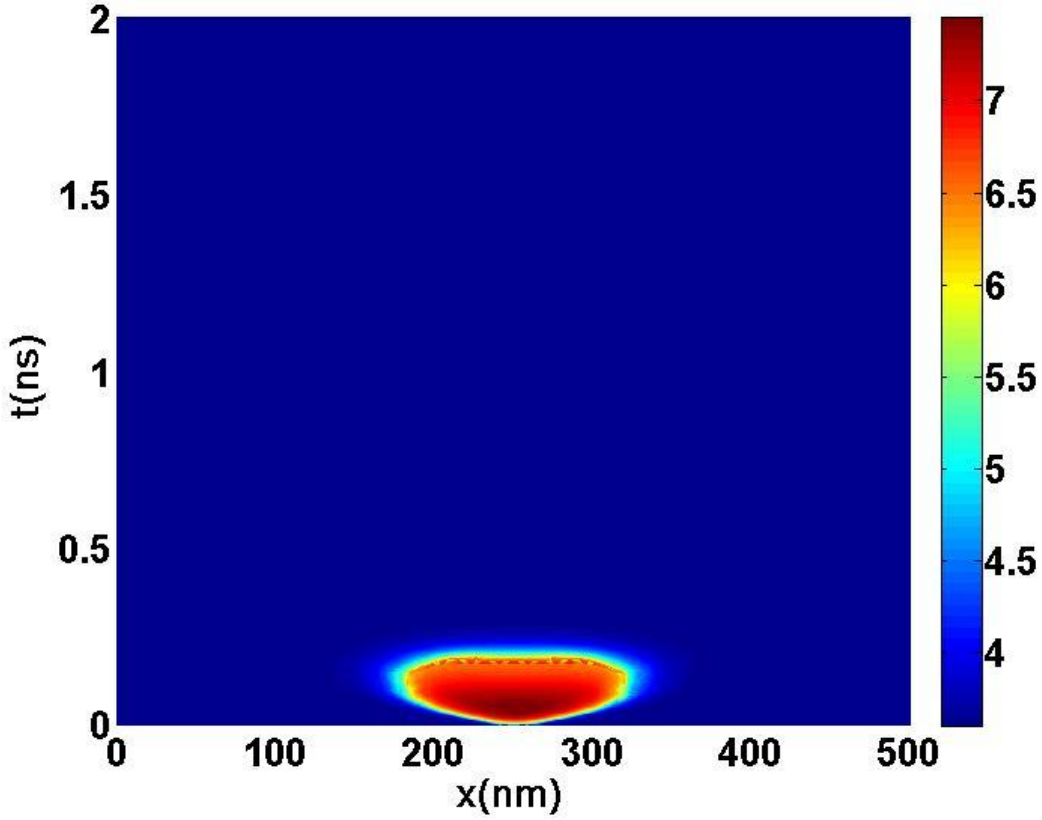

Figure 26 80 nm Nanowire with a series kinetic inductance of 150 nH.

An extra inductance was added (compared to figure 24) to simulate how much the pulse width would increase with increasing inductance. This is done because the bad results in (5.6) were suggested to come from the fact that the pulse width was too short to measure with the used frequency counter.

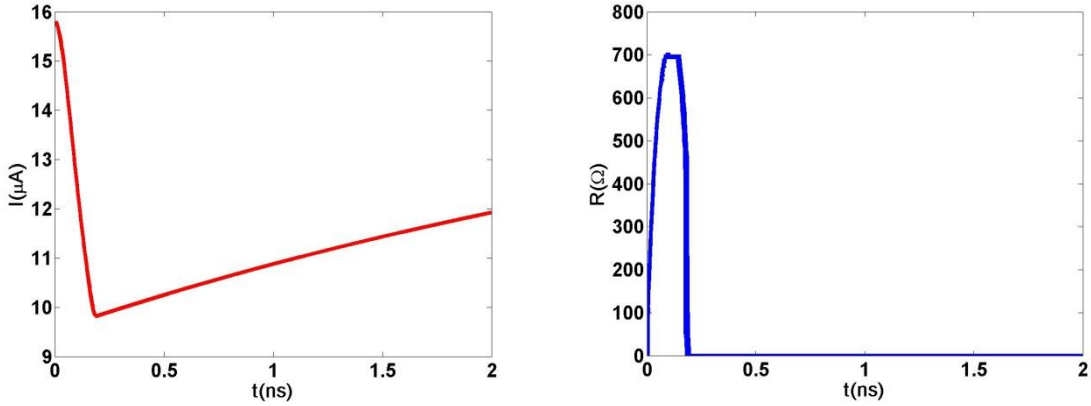

Figure 27 Current through and resistance of an 80 nm nanowire with an extra series kinetic inductance.

In figure 26 and 27, a 80nm nanowire is simulated with a series kinetic inductance. This inductance causes the hotspot size to increase initially, but also causes the current through the nanowire to increase slower. This gives the nanowire more time to dissipate the heat before the current starts to heat the nanowire up again. The nanowire now has more time to become superconducting again.

There are some measurements performed on three narrow types of nanowire and it is concluded that they are indeed functioning properly. However, since the time for the experiments is too short, further measurements are needed in the future to get more results and to be able to compare results optically. This comparison is going to give better understanding about the quality of the films for the purpose.

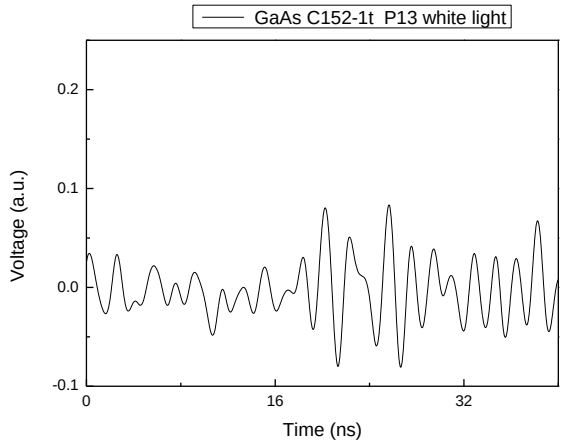

a) An oscilloscope trace with the white light focused on the 80 nm nanowire. There are no peaks visible

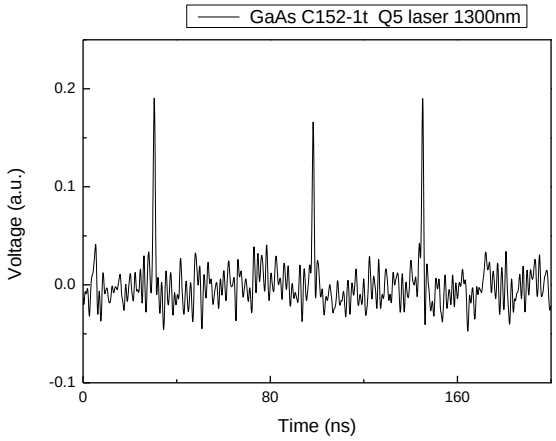

b) A 1300 nm laser is focused on the nanowire. Now there are some clear pulses visible.

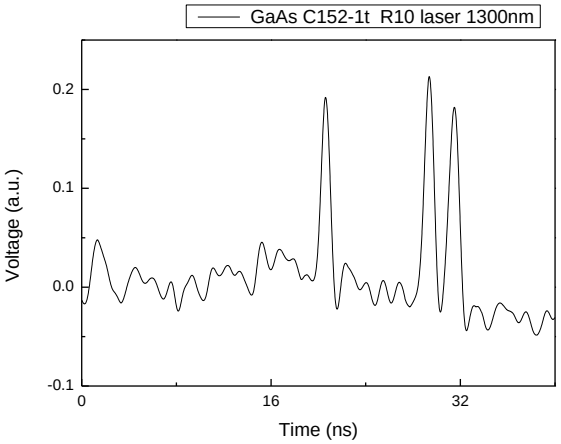

c) Oscilloscope trace of a few voltage pulses in more detail.

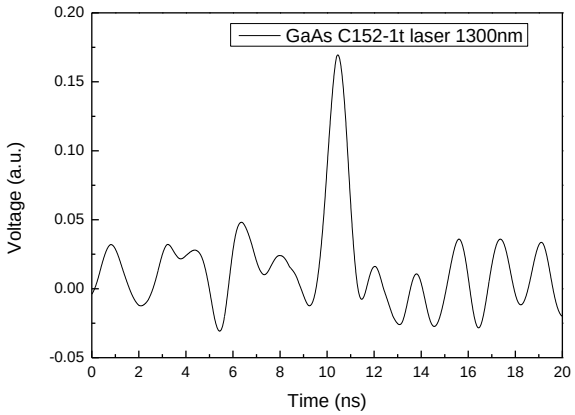

d) close up of a single voltage pulse. The width is approximately 2 ns, which coincides with the results from the simulations in figure 25.

Figure 28 Oscilloscope images of the optical measurements on nanowires between 90 and 130 nm wide.

In figure 28, the voltage pulses are plotted against the time. From these images, it can be concluded that the narrower nanowires are working as desired; however, more measurements have to be performed in the future to be able to analyze and compare the results.

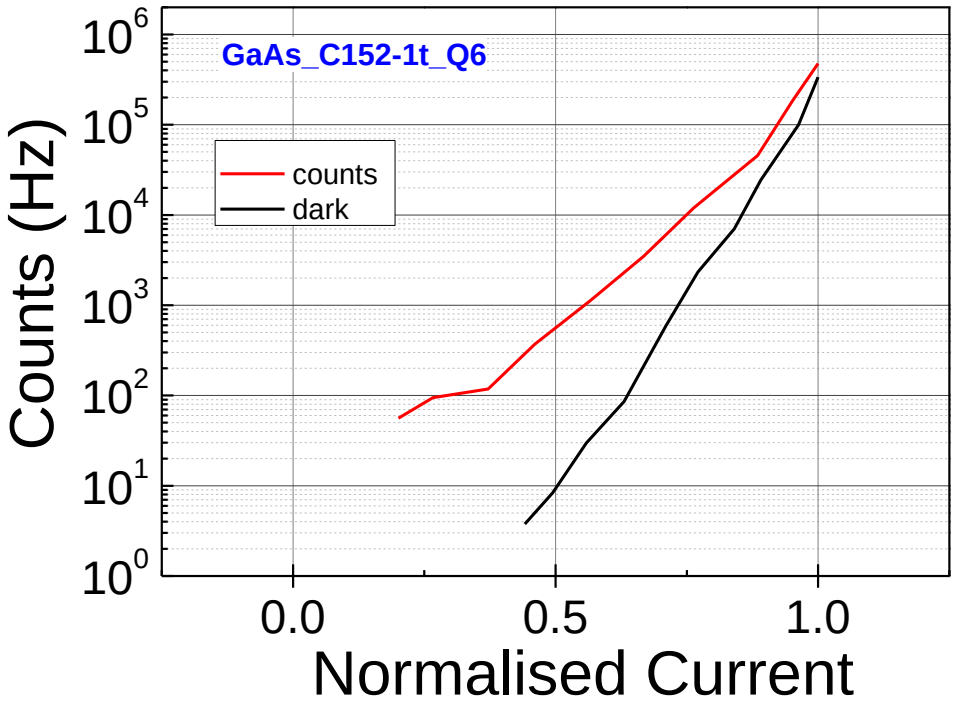

Figure 29 Count versus normalized current. The laser power on the sample is approximately 200 nW.

In figure 29, the dark count and the light count (with laser off and on respectively), are represented in number of counts against the normalized current. The normalized current is the bias current divided by the critical current of the nanowire. From the graph, it is clear that there are less counts for dark measurements than when the laser is turned on. This is to be expected, as the laser light has much more photons directed at the sample inducing more photon absorptions. The difference between dark and light counts decreases as the bias current approaches the critical current. This is because the dark count rate increases faster than the efficiency with increasing bias current. [13]

.

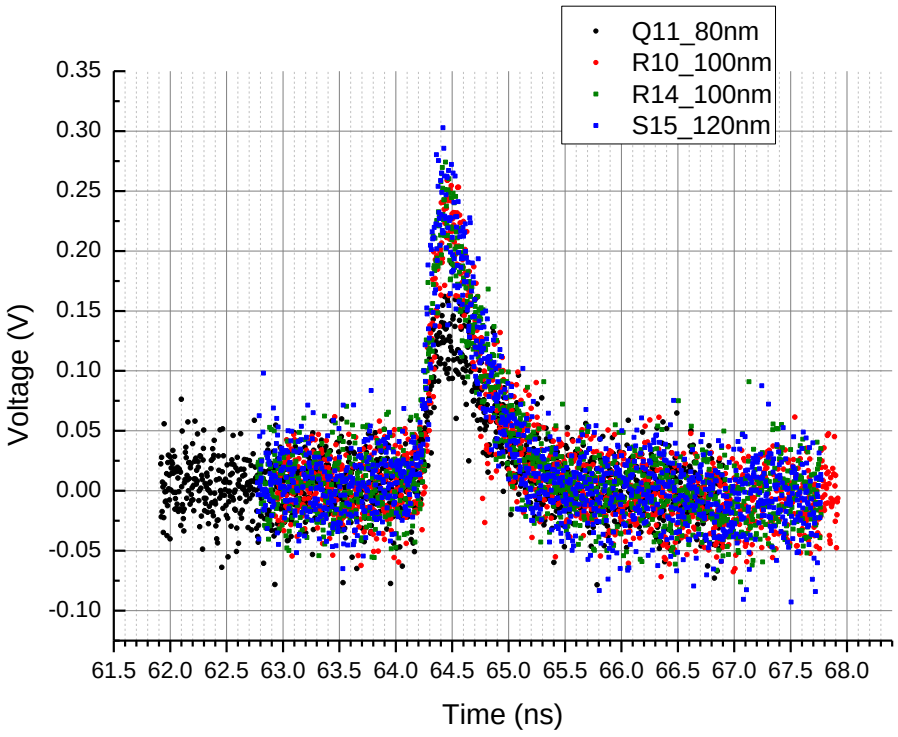

Figure 30 Sampling oscilloscope image to retrieve the pulse shape.

In figure 30, an image result from the sampling oscilloscope is plotted. There are four different wires measured and the pulse shape of those wires is plotted together. This shows that the pulses are the same in shape and magnitude. From the graph, it can also be deduced that the fall time (time between maximum voltage and zero voltage) is about one nanosecond.

6 Conclusion

The samples used in these experiments are the first real processing on NbN films grown at TU/e. The goal of this project was to analyze the quality and performance of the nanowires grown from the NbN films. To do this, the actual widths were measured using SEM . This showed that the actual widths are different from the desired widths. It also showed why several devices were not working. This was caused by broken wires, bad connections between the nanowire and the contact pad or the fact that there was no nanowire at all.

Then, the room temperature resistance was measured, mainly to see if the devices were working. Then, at low temperature, the resistance was measured again, and a characteristic IV curve was made for every working device. From this, the stability of the hotspot could be deduced and also the critical current could be extracted.

Several different methods were then used to perform a statistical analysis on the devices. This showed that the I_cR_n method did account for some physical constrictions working on the whole nanowire. The deviation compared to the average was generally lower for the I_cR_n method compared to the J_c method.

The RRR analysis showed that there are quite some differences in the pollution levels of the samples. The concentration of nitrogen compared to Niobium will contribute most to this.

The optical measurements performed, were insufficient to say anything about the quality of the different devices or the performance of the devices. However, they did show that the narrow nanowires are working properly and can be used as single photon detectors. The simulations confirmed that the 500 nm nanowires are indeed latching.

Images made with the sampling oscilloscope were used to identify the pulse shape. This shape was the same for the different working nanowires.

7 Acknowledgement

This project would not have been possible without the help of other people. Because of this I would like to thank them for all the help and support they provided during my internship. I would first like to thank Döndü Sahin, for all the time and effort she put into helping me with the experiments, explaining how the experiments work, and being available whenever there were questions about the project. I would also like to thank Prof. dr. Andrea Fiore, for his help and ideas, especially when the results during the project were unexpected. Saeedeh Jahanmirinejad, I would like to thank for providing and explaining the electro-thermal model. Last, but definitely not least, I would like to thank Jos Bremmers for providing all the helium required for the experiments.

I would also like to thank everybody else who was in any way helpful and/or supporting during this project.

8 Literature

[1] Francesco Marsili, "Single-photon and photon-number-resolving detectors based on superconducting nanowires", PhD thesis, 2009.

[2] J. E. Mooij, in "Percolation, Localization, and Superconductivity", Plenum Press, New York, 1984, p. 325.

[3] Joel K. W. Yang, "Modeling the Electrical and Thermal Response of Superconducting Nanowire Single-Photon Detectors", IEEE transactions on applied superconductivity, 2007, vol. 17, no 2, p 581-585.

[4] http://www.ifn.cnr.it/Groups/SQC/index.htm

[5] Eric Dauler, "Multi-element Superconducting Nanowire Single Photon Detectors", Applied superconductivity, 2007, Vol. 17, issue 2, MIT, PhD thesis.

[6] Eric Dauler, "1.25-Gbit/s photon-counting optical communications using a two-element superconducting nanowire single photon detector", Advanced photon counting techniques, 2006, vol. 6372.

[7] Jin Zhang, "Response time characterization of NbN superconducting single photon detectors", Applied superconductivity, 2003, vol. 13, no. 2, p 180-183.

[8] G.N. Gol'tsman, "Fabrication of nanostructured superconducting single photon detectors", Applied superconductivity, 2003, vol. 13, no. 2, p192-195.

[9] S. Adam, "Discontinuous hotspot growth related to the thermal healing length in superconducting NbN microstrips, Journal of physics: conference series 234, 2010.

[10] F.Mattioli, "Electrical characterization of superconducting single-photon detectors", Journal of applied physics, 2007 vol. 101, 054302.

[11] F. Marsili, "afterpulsing and instability in superconducting nanowire avalanche photodetectors", Applied Physics Letters, 2012, Vol. 100, Issue 11, id. 112601 (5 pages).

[12] Chandra M Natarajan, "Superconducting nanowire single photon detectors: physics and applications", Superconductor science and technology, 2012, vol 25, p1-16.

[13] G.S. Buller, "Single photon generation and detection", Measurement science and technology, 2010, vol. 21, 28pp.

[14] A.D. Semenov, G.N. Gol'tsman, "Quantum detection by carrying superconducting film", Physica C, 2001, vol. 351, p 349-356.

[15] G.N. Gol'tsman, "Picosecond superconducting single photon optical detector", Applied physics letters, 2001, vol. 79 no. 6, p705-707.

[16] D.J. Griffiths, "Introduction to quantum mechanics", second edition, 2004.

[17] A. Semenov, "Optical and transport properties of ultrathin NbN films and nanostructures", PRB, 80,054510, 2009.

9 Appendix

9.1 IV curves

The IV curves for different widths for a all samples are shown in the graphs below.

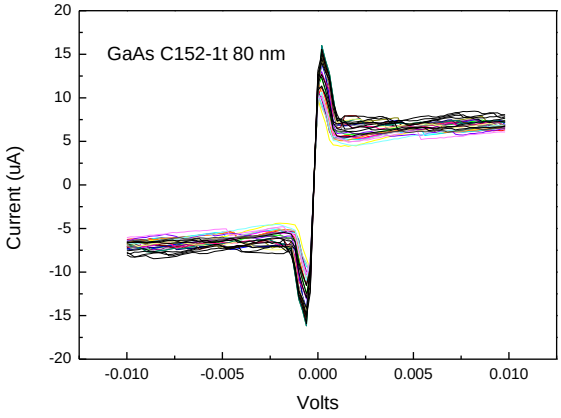

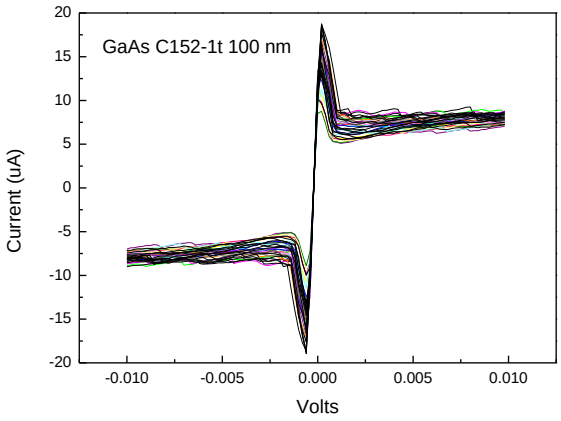

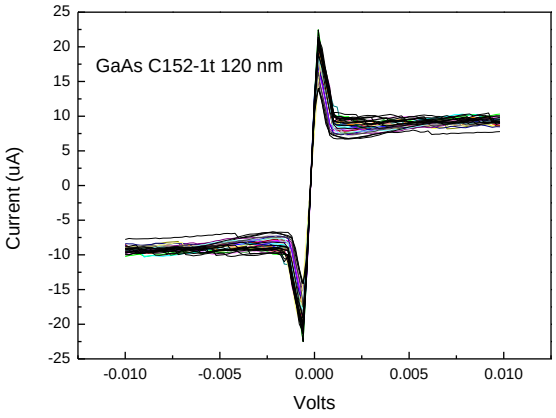

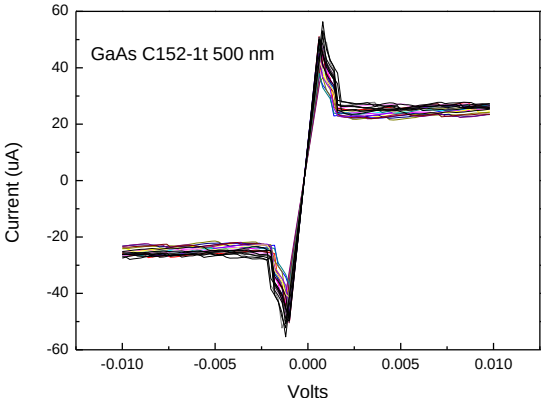

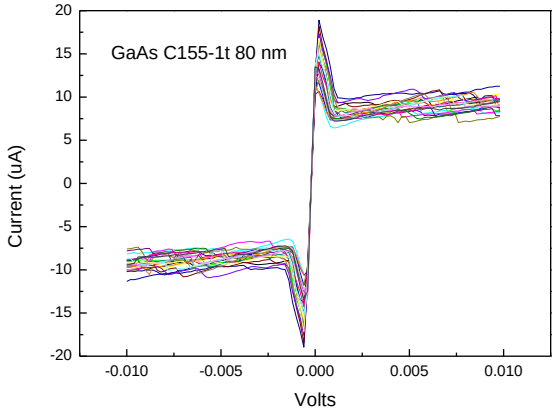

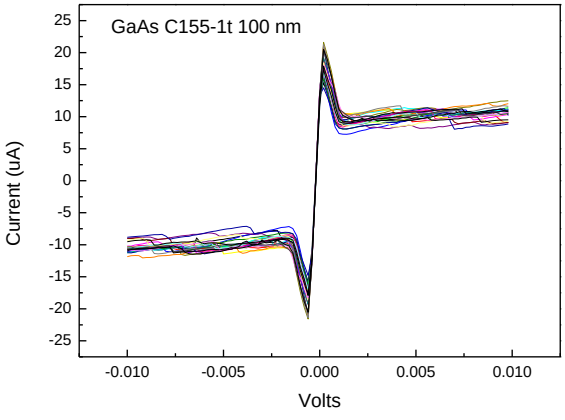

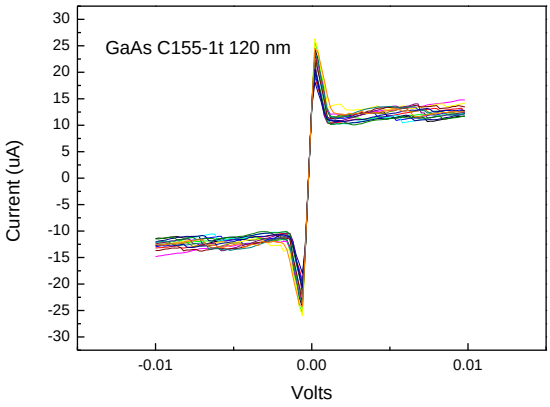
GaAs C155-1t 120 nm
Current (uA)
Volts

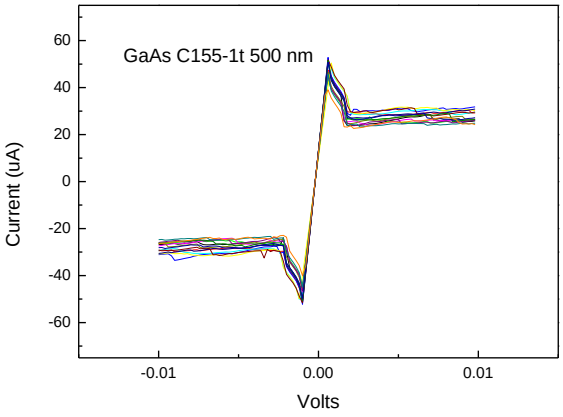
GaAs C155-1t 500 nm
Current (uA)
Volts

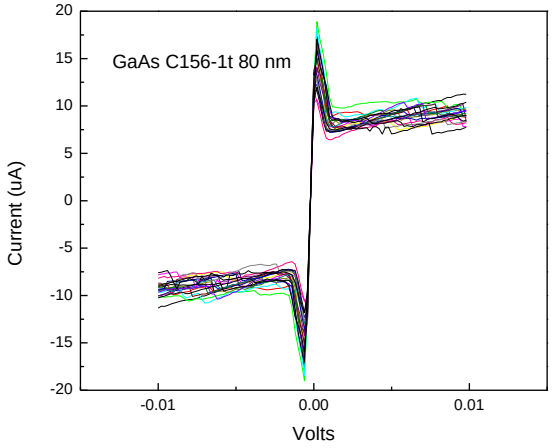
GaAs C156-1t 80 nm
Current (uA)
Volts

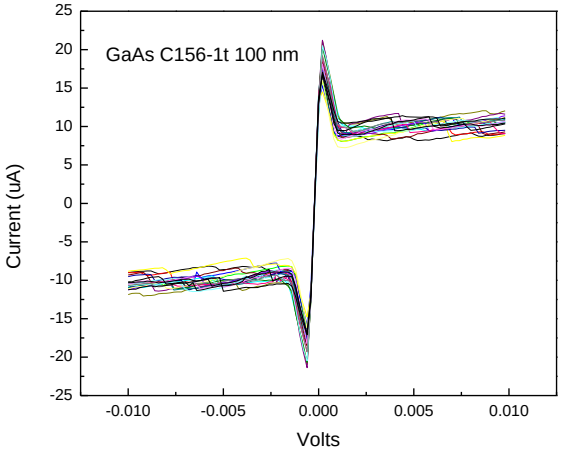
GaAs C156-1t 100 nm
Current (uA)
Volts

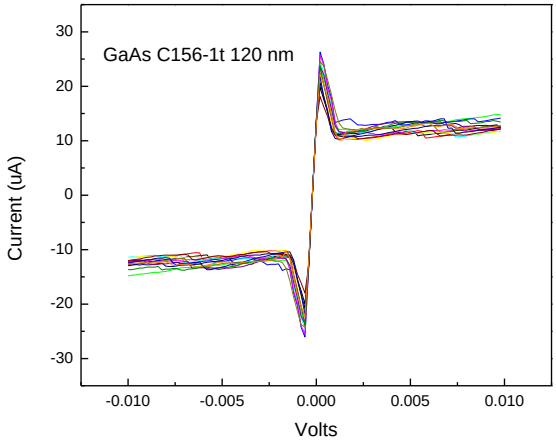
GaAs C156-1t 120 nm
Current (uA)
Volts

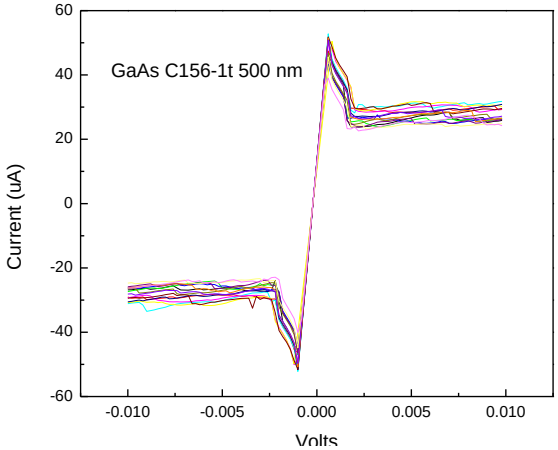
GaAs C156-1t 500 nm
Current (uA)
Volts

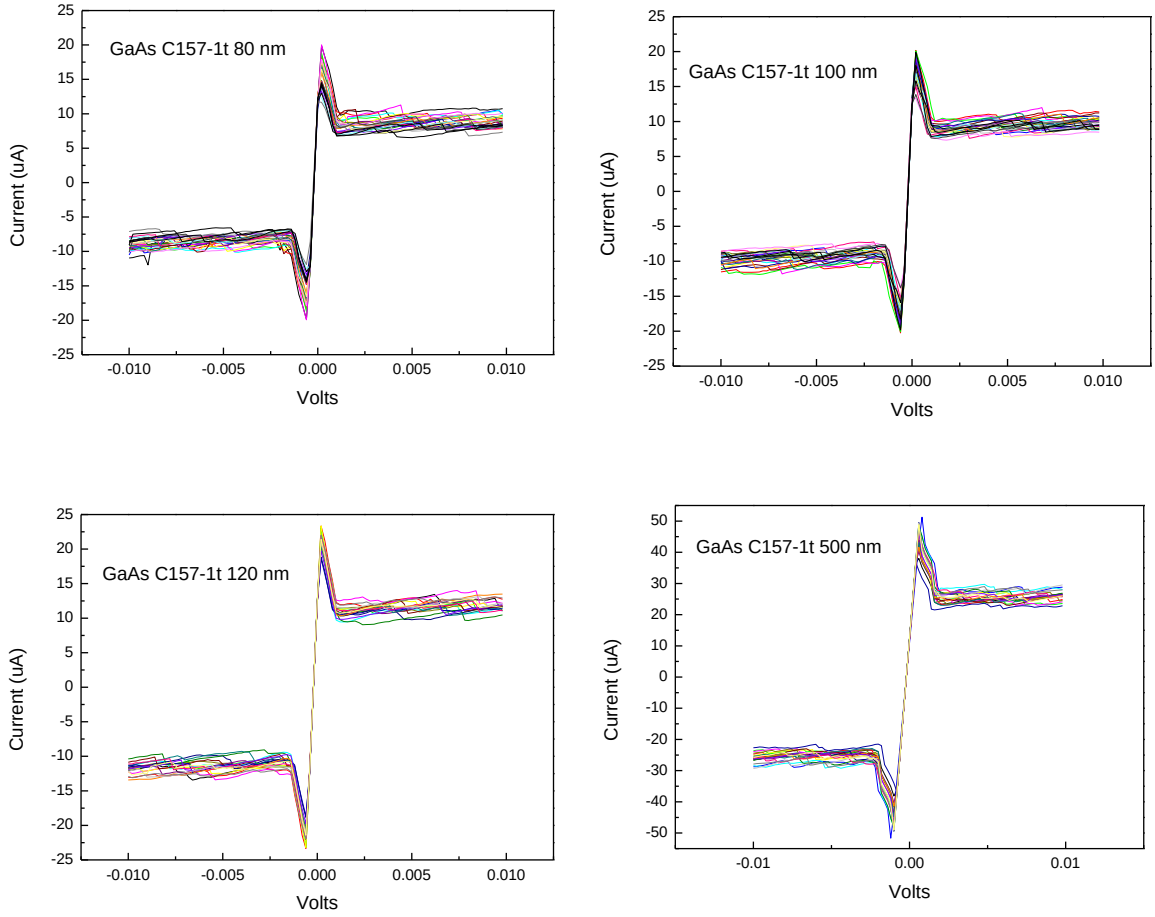

Figure 31 The IV curves of all widths of all four samples. The respective sample name and nanowire width is denoted on every graph.

9.2 I_cR_n graphs

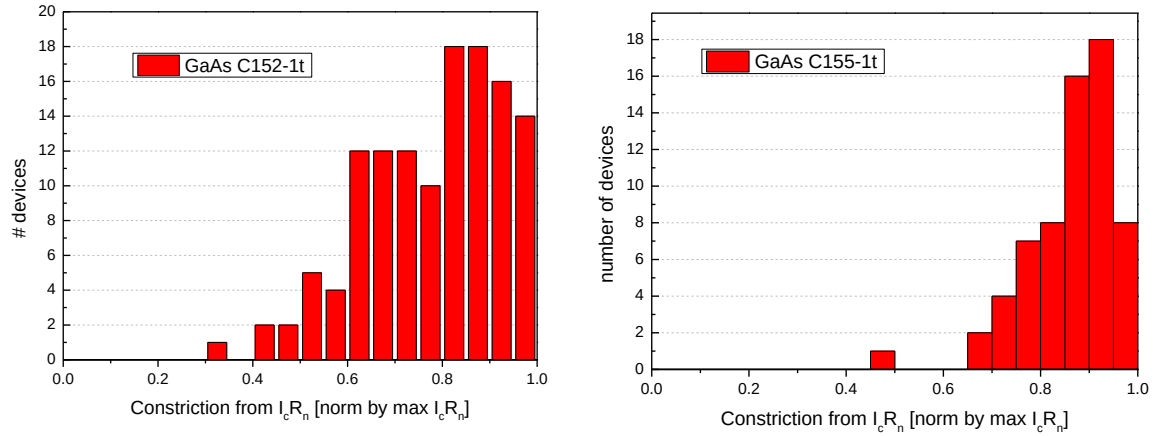

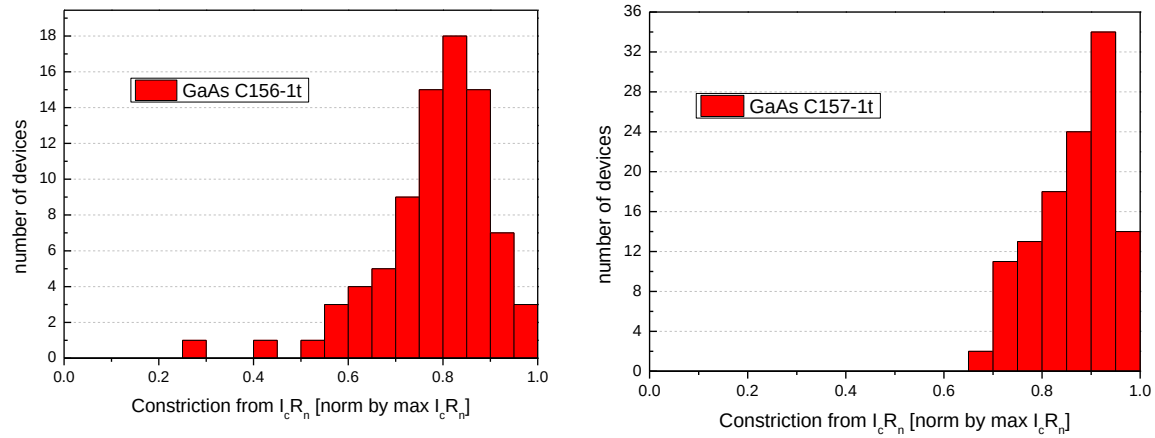

Figure 32 The I_cR_n analysis for every sample separately.

9.3 J_c graphs

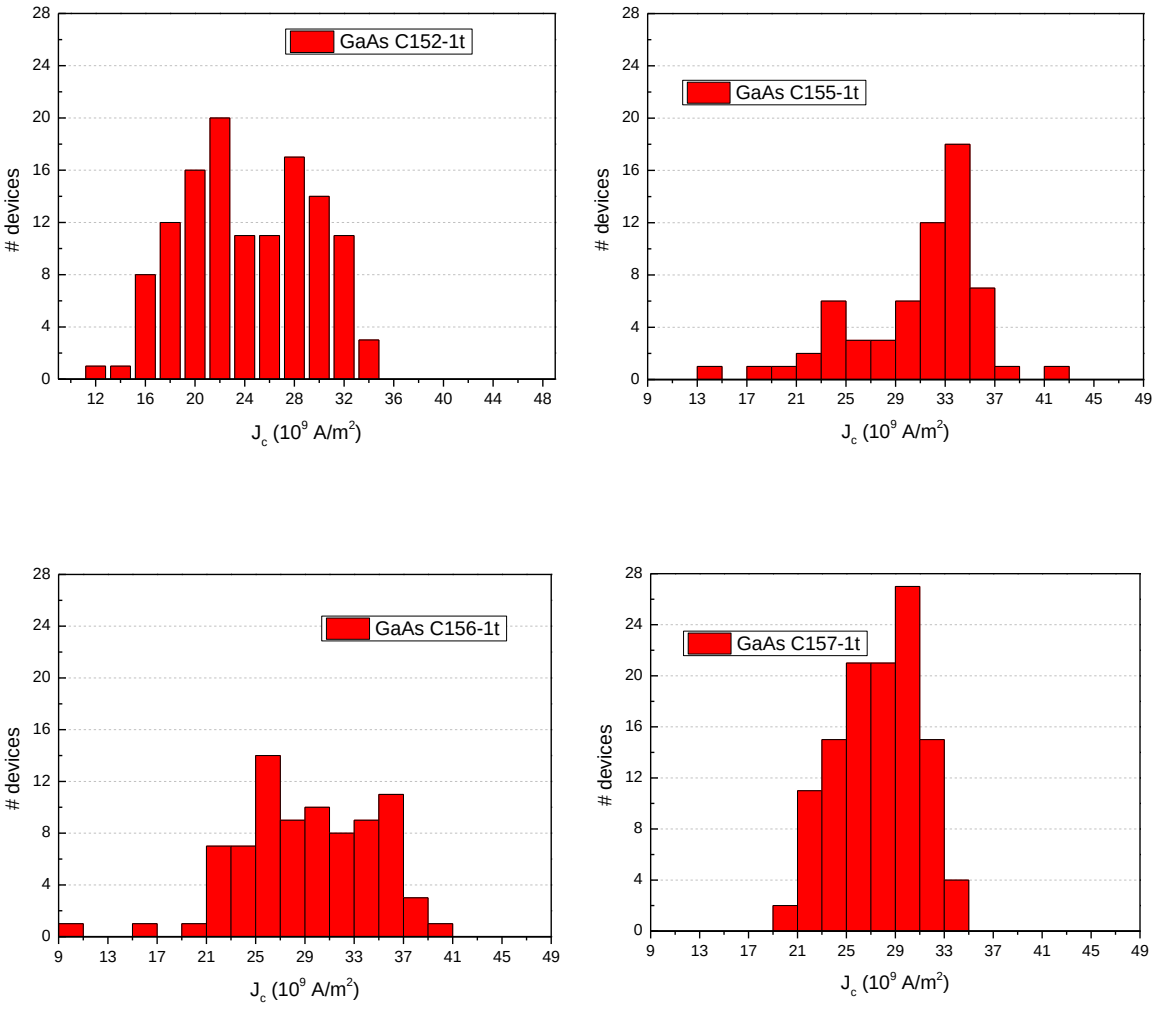

Figure 33 The J_c statistics for every sample separately.

9.4 Data table

Sample name	Width (nm) →	80			100			120			500			Total		
	Ic (uA) and Jc (10^9 A/m^2) →	Ic	IcRn	Jc	Ic	IcRn	Jc	Ic	IcRn	Jc	Ic	IcRn	Jc	Ic	IcRn	Jc
C152-1t	Average	12.28	0.729	23.23	14.44	0.738	24.56	18.89	0.882	29.35	46.69	0.713	19.53	/	0.780	24.25
	Standard deviation	2.12	0.188	4.00	2.73	0.149	4.64	2.10	0.134	3.29	5.35	0.139	2.24	/	0.144	5.16
	Percentage	17.30	16.22	17.20	18.89	20.23	18.89	11.13	15.14	11.20	11.45	19.48	11.45	/	18.47	21.29
														/		
C155-1t	Average	16.38	0.784	29.63	18.58	0.815	28.65	25.21	0.919	33.60	49.83	0.849	23.25	/	0.862	30.87
	Standard deviation	2.13	0.078	3.86	3.37	0.123	5.20	1.02	0.038	1.37	5.96	0.069	2.78	/	0.095	5.10
	Percentage	13.01	9.95	13.02	18.14	15.14	18.14	4.06	4.13	4.06	11.96	8.19	11.96	/	11.04	16.51
														/		
C156-1t	Average	14.09	0.697	27.92	18.23	0.803	31.52	21.74	0.826	32.63	48.90	0.838	24.76	/	0.785	29.11
	Standard deviation	2.64	0.125	5.24	3.20	0.125	5.53	2.35	0.082	3.52	3.11	0.032	1.58	/	0.120	5.45
	Percentage	18.76	18.0	18.76	17.55	15.55	17.55	10.80	9.94	10.80	6.37	3.76	6.37	/	15.35	18.71
														/		
C157-1t	Average	15.66	0.842	26.56	17.42	0.862	28.23	21.20	0.889	29.38	45.61	0.871	24.49	/	0.866	27.52
	Standard deviation	2.02	0.084	3.43	1.90	0.080	3.08	1.44	0.044	1.99	4.08	0.066	2.19	/	0.076	3.36
	Percentage	12.93	9.98	12.93	10.9	9.30	10.90	6.79	5.00	6.79	8.95	7.54	8.95	/	8.75	12.21

Table 7 Table containing the average, standard deviation and percentage of every type of nanowire for all samples.